



# Fluid Behavior in Nanoporous Silica

Salim Ok<sup>1\*</sup>, Bohyun Hwang<sup>1</sup>, Tingting Liu<sup>1</sup>, Susan Welch<sup>1</sup>, Julia M. Sheets<sup>1</sup>, David R. Cole<sup>1,2</sup>, Kao-Hsiang Liu<sup>3</sup> and Chung-Yuan Mou<sup>4</sup>

<sup>1</sup> School of Earth Sciences, The Ohio State University, Columbus, OH, United States, <sup>2</sup> Department of Chemistry, The Ohio State University, Columbus, OH, United States, <sup>3</sup> Shull Wollan Center-A Joint Institute for Neutron Sciences, Oak Ridge National Laboratory, Oak Ridge, TN, United States, <sup>4</sup> Department of Chemistry, National Taiwan University, Taipei, Taiwan

We investigate dynamics of water (H<sub>2</sub>O) and methanol (CH<sub>3</sub>OH and CH<sub>3</sub>OD) inside mesoporous silica materials with pore diameters of 4.0, 2.5, and 1.5 nm using low-field (LF) nuclear magnetic resonance (NMR) relaxometry. Experiments were conducted to test the effects of pore size, pore volume, type of fluid, fluid/solid ratio, and temperature on fluid dynamics. Longitudinal relaxation times (T<sub>1</sub>) and transverse relaxation times (T<sub>2</sub>) were obtained for the above systems. We observe an increasing deviation in confined fluid behavior compared to that of bulk fluid with decreasing fluid-to-solid ratio. Our results show that the surface area-to-volume ratio is a critical parameter compared to pore diameter in the relaxation dynamics of confined water. An increase in temperature for the range between 25 and 50°C studied did not influence T<sub>2</sub> times of confined water significantly. However, when the temperature was increased, T<sub>1</sub> times of water confined in both silica-2.5 nm and silica-1.5 nm increased, while those of water in silica-4.0 nm did not change. Reductions in both T<sub>1</sub> and T<sub>2</sub> values as a function of fluid-to-solid ratio were independent of confined fluid species studied here. The parameter T<sub>1</sub>/T<sub>2</sub> indicates that H<sub>2</sub>O interacts more strongly with the pore walls of silica-4.0 nm than CH<sub>3</sub>OH and CH<sub>3</sub>OD.

**Keywords:** low viscous fluids, confined state, relaxation, low-field NMR, subsurface

## OPEN ACCESS

### Edited by:

Doo Soo Chung,  
Seoul National University, South Korea

### Reviewed by:

Bin Ding,  
Donghua University, China  
Ahmet Akin Uenal,  
Max Born Institute for Nonlinear  
Optics and Short-Term Spectroscopy  
(LG), Germany

### \*Correspondence:

Salim Ok  
sok@uos.de

### Specialty section:

This article was submitted to  
Physical Chemistry and Chemical  
Physics,  
a section of the journal  
Frontiers in Chemistry

**Received:** 08 October 2019

**Accepted:** 16 July 2020

**Published:** 28 August 2020

### Citation:

Ok S, Hwang B, Liu T, Welch S,  
Sheets JM, Cole DR, Liu K-H and  
Mou C-Y (2020) Fluid Behavior in  
Nanoporous Silica.  
Front. Chem. 8:734.  
doi: 10.3389/fchem.2020.00734

## INTRODUCTION

There has been enormous interest in understanding the behavior of nanoconfined fluids due to its relevance in various areas such as biology and geochemistry (Vogel, 2010; Millischuk and Ladanyi, 2014). The behavior of molecules in confined geometries differs significantly from bulk behavior (Vogel, 2010; D'Agostino et al., 2012). This deviation arises from several factors including the relation between fluid and nanoporous matrix, and the effects of the size, shape, and geometry of the solid matrix on fluid behavior (Vogel, 2010; D'Agostino et al., 2012; Millischuk and Ladanyi, 2014). The issues on physical and chemical properties of confined fluids are heavily discussed (D'Agostino et al., 2012; Mallamace et al., 2014) along with the characterization of mesoporous solids with precise pore structure (Webber and Dore, 2004). Fundamental understanding of porous systems and their interaction with confined liquids is essential because mesoporous solids are used as model systems relevant to geological materials in the subsurface and have applications in separations, nanofluids, and catalysis (Millischuk and Ladanyi, 2014).

Mesoporous silica systems are a group of nanoporous materials with distinct cylindrical mesochannels, easily adjustable pore sizes, large surface areas, and even tunable particle sizes and shapes (Asefa and Tao, 2012). These mesoporous materials have generated interest because of their possible uses as supports for practical innovative materials (Al-Othman, 2012). Due to their large surface areas, these engineered proxies are ideal nanoporous systems for exploring confined fluid

behavior at pore surfaces. For porous silica glasses, various degree of pore filling as compared to total pore volume of the nanoporous material with distilled water have been investigated with both relaxation and diffusion NMR approaches (Bhattacharya et al., 1989; D’Orazio et al., 1990a,b). Both longitudinal ( $T_1$ ) and transverse ( $T_2$ ) relaxation measurements showed a linear relationship with respect to fluid filling equivalent to monolayer coverage. This arises from the homogeneity of nanopores where the water molecules are evenly distributed. In the current study, we provide detailed characterization on the properties of mesoporous materials and discuss how the properties of these mesoporous materials influence the dynamics of confined fluids.

There are contradictory conclusions on the confined fluid behavior of nanoporous systems. For instance, D’Agostino et al. (2012) observed that diols, such as ethylene glycol and 1,2-propanediol, showed increased diffusivity within the pore space of titania (22 nm average pore size) and silica (13 nm average pore size) compared to alkanes including n-hexane and n-octane.  $T_1$  measurements also demonstrated that tumbling rate of polyols was not influenced by the porous medium while there was a significant drop of  $T_1$  for the alkanes. Among confined fluids, water has central significance for gaining insight into a wide range of systems including various geological and technological materials. In general, despite large number of literature work on confined water, the behaviors such as diffusion property of water in confined geometry is not fully understood (Ricci and Rovere, 2000; Swenson et al., 2001). The contradictory results are attributed to different factors such as competition between confinement and surface effects, dependence on temperature, and the characteristics of the surface interactions-hydrophilic vs. hydrophobic (Swenson et al., 2001). Experimental studies on water showed decreasing motion with increasing confinement for various surface substrates (Bellissent-Funel et al., 1995; Denisov and Halle, 1996; Zanotti et al., 1999). Contradictory results, such as an extensive hydrogen bonded network of water close to the surface (Steytler and Dore, 1985) vs. a reduction in number of hydrogen bonds per water molecule near cavity walls (Bruni et al., 1998) have been observed. Besides that, the influence of confinement is less pronounced in two-dimensional substrate type confinements than in three-dimensional confinements such as pores (Barut et al., 1998; Bergman and Swenson, 2000). Because of the controversial interpretations of the behaviors of confined fluids and water in particular, there is still a need to probe the molecular-level behavior of fluids as a function of a number of key parameters including, but not limited to, pore size, pore volume, fluid type, fluid-to-solid ratio, and temperature. In addition, conducting research on simple fluids such as water in confined state and developing models on confined behavior of low viscous fluids could be extended and utilized for better experimental design and understanding of complex fluids under confinement. For instance, mesoporous silica type materials are of special interest in crude oil industry, and these materials are ideal engineering proxies to investigate larger organic molecules such as decalin and tetradecane, and their mixtures to mimic a micro-environment resembling a petroleum aromatic fraction (Kapoor et al., 2000) under confinement.

The novelty of the current work is studying dynamical behavior of fluids in confined states systematically by varying fluid volume, temperature, and pore diameter of the confining solid to better understand complex heterogeneous subsurface systems. These include fluids such as water and hydrocarbons in rock that have various wetting behaviors in the subsurface. The remarkable aspect of the mesoporous silica materials used in the present study is the utilization of them as catalyst materials in petroleum industry. Therefore, the projection of this work will be to extend the current efforts in terms of investigating more complex mixtures of fluids under confinement. In order to focus on that, first emphasis is showing distinguishability of confined vs. bulk-like fluids.

Our approach to distinguish the signals of fluids between confined and bulk-like states in different pore networks may have applications in rock core analysis using low-field NMR. To this end, in addition to using nanoporous silica powder, nanoporous silica rods (monolith samples) also were used, allowing for the study of confinement of water without excess water. Excess water has been observed in the case of mixtures of white powder nanoporous silica with water upon centrifugation, and it is bulk-like water. However, in the case of silica rods, there is no excess water outside the rod itself. First, the dynamical behaviors of bulk fluids in an NMR were determined by NMR relaxation measurements. Then the same NMR measurements were conducted on nanoporous silica powders having *confined* fluid (fluid in mesoporous silica and fluid interacting with the pore walls), as well as fluid in the interparticle regions of nanoporous silica powder and outside the pores, and *excess* fluid (fluid observed upon centrifugation of mixtures of nanoporous silica and fluids and showing bulk-like dynamical behavior). Hence, we aim to achieve the following goals: (i) to characterize the nanoporous silica systems in detail, (ii) to determine the degree of deviation of confined fluid behavior with respect to bulk fluid, (iii) to clarify the influence of pore parameters to the deviation of confined fluid behavior from bulk, and (iv) to show how to differentiate signals of confined fluid in nanopores from excess fluid.

## MATERIALS AND METHODS

### Samples

Mesoporous silica with mean nanopore diameter and particle size of 4 and 200 nm, respectively, was purchased from Sigma-Aldrich. The silica porous monolith samples with nominal pore diameter of 5.0 nm, total pore volume of 0.7 cm<sup>3</sup>, specific density of 1.1 cm<sup>3</sup>, and BET surface area of 580 m<sup>2</sup>/g were purchased from Particle Solutions, LLC (Alachua, FL). Silica-1.5 nm was prepared by calcination of micellar template silica matrices made up of micrometer size grains. Pre-formed  $\beta$ -zeolite kernels (composed of tetraethylammonium hydroxide), NaOH, and fumed silica reacted with decylmethylammonium bromide solution in order to synthesize the silica matrix (Liu et al., 2013). The  $\beta$ -zeolite seeds were utilized to make the silica nanopore walls semi-crystalline and resilient to hydrolysis deterioration (Liu et al., 2000). The mixture was first relocated into an autoclave at 120°C for 2 days, then decreased to room temperature while

adjusting the pH to 10. Upon sealing in an autoclave at 100°C for 2 days, the probe was accumulated by filtration in solid state, washed by water and ethanol, and dried at 60°C in air overnight. The ultimate mesoporous silica was obtained by calcination at 540°C for 8 h (Liu et al., 2013). Silica-2.5 nm was produced by an analogous procedure. The minor difference was the utilization of different carbon chain length surfactants or hydrothermal curing (Liu et al., 2013). Both silica-2.5 nm and silica-1.5 nm are cured with the second hydrothermal treatment; hence have even stronger structure and better hydrolysis resilience. Liu et al. (2006) provides further description on the synthesis of these two samples of silica-2.5 nm and silica-1.5 nm. It should be emphasized that the determined pore diameters of the samples in the present study are average values.

## Characterization

Pore size, pore volume, and surface area measurements were made with a Micromeritics ASAP 2020 gas sorption analyzer. The mesoporous silica samples were degassed at 423 K for 20 h under a vacuum pressure of 10  $\mu$ m Hg to eliminate the impurities and gases within the pores. Nitrogen was the adsorbate used to acquire the adsorption and desorption isotherms at 77 K (see **Table S1** and **Figure S1** in Supporting Information). Transmission X-ray diffraction (TXRD) experiments were conducted with a PANalytical X'Pert Pro diffractometer. Transmission geometry permits accurate and precise measurement at the low  $2\theta$  angle range required for obtaining the long-range ordered pore structure. A thin layer of specimen was mounted between two films of Kapton foil to reduce beam absorption. TXRD measurements on nanoporous silica-4.0 nm and silica-1.5 nm were acquired using Cu K $\alpha$  radiation and an X'Celerator detector. Data were acquired from 1 to 43°  $2\theta$ , with a step size of 0.02°  $2\theta$  and a speed of 20 s/step. Applied voltage and tube current for the measurements were 45 kV and 40 mA. TXRD measurement on silica-2.5 nm was acquired using a scintillation detector. Data were collected from 1 to 15°  $2\theta$ , with a step size of 0.02°  $2\theta$  and a speed of 12 s/step. Applied voltage and tube current for the measurements were 45 kV and 40 mA (see **Figures S2a–c**) for TXRD scans of nanoporous silica samples).

Samples for thermogravimetric analysis (TGA) measurements were prepared by blending 150 mg of each silica sample with 1.0 ml distilled water in a 4 ml clear vial. The mixtures were kept at 20°C for a week for complete saturation of the pores with water. After centrifugation of the samples for 20 min at 5,000 rpm on an Eppendorf Centrifuge 5340 V 4.4, supernatant was taken. The samples were left again overnight after stirring with small glass rods. This procedure of centrifugation, removal of supernatant, and overnight keeping were repeated at least 10 days to make it sure that no excess water was left between the grains. Then water saturated porous silica samples were dried under continuous flow of neat air for durations ranging from 5 to 85 min. Successively, 10–20 mg samples were placed into a Pt crucible. Finally, the TGA measurements were run on a Perkin Elmer TGA7 Thermogravimetric Analyzer from 25 to 900°C under the flow of nitrogen gas with a flow rate of 15 ml/min and a heat rate of 20°C/min (see **Figures S3a,b** showing the TGA

results). TG curves of silica samples prepared by different drying times exhibit weight loss behavior. The weight losses correspond to the elimination of water, and hence pore volume comparison of the mesoporous silica materials.

## Sample Preparation for Low-Field NMR Measurements

Hundred and fifty milligrams of each mesoporous silica sample were filled with three different amounts of distilled water 0.8, 0.6, and 0.4 ml. The samples were left overnight at least prior to conducting measurements for complete filling of the pores (see **Figures S4a–e**) in supporting information showing the photos of excess water after centrifugation and homogenization by sonication). For confining CH<sub>3</sub>OH and CH<sub>3</sub>OD, silica-4.0 nm was mixed with 0.9, 0.6, and 0.4 ml of each of these fluids. As with water, the samples were left overnight at minimum prior to conducting measurements to ensure complete filling of the pores. The samples were capped to prevent evaporation. Each sample was homogenized by sonication for 15 min immediately prior to the low-field NMR measurements. Controlled measurements were done to distinguish excess fluid signal from confined fluid signal (see **Figures S4a–e**). As seen in **Figure S4**, this was achieved by centrifugation of samples for 20 min at 5,000 rpm so that excess water migrated on top of the silica and water mixture (see **Table 1** for the summary of the experimental conditions of the samples).

A second set of samples was prepared as follows: 218.0 mg silica-4.0 nm, 100.0 mg silica-2.5 nm, and 173.0 mg silica-1.5 nm were mixed with 0.4 ml deionized H<sub>2</sub>O. This adjustment was made to keep the pore volume of each nanoporous silica powder consistent around 120 cm<sup>3</sup>, for a given amount of surface area (see **Table 2** for detailed values). The samples were left for soaking overnight at minimum prior to the measurements to ensure complete pore fillings. The samples were sonicated for 15 min to homogenize throughout the sample right before the measurements. The measurements were conducted at 313 K.

The third set of samples was prepared using porous silica monolith samples that were thermally treated overnight at 400°C to remove moisture and any organics left from the synthesis of the monolith samples. Upon cooling to 25°C, the samples were soaked in water for 10 min, measured and then soaked until 90 min. Visual inspection showed that the sample soaked for 10 min had non-transparent region in the middle of the sample, while such a region was not seen in the sample soaked for 90 min. This non-transparent region is attributed to volume not filled with water.

## <sup>1</sup>H Low-Field NMR Relaxometry Measurements

Low-field NMR T<sub>1</sub> and T<sub>2</sub> relaxation measurements were performed on a Bruker Minispec mq20 NF Series instrument with a magnetic field strength of 0.47 T equivalent to a proton resonance frequency of 20 MHz (see **Table 1** showing the details of experimental conditions), and the data were acquired utilizing Minispec software. The instrument contains a 10 mm temperature-variable probe. Temperature control is

**TABLE 1** | Experimental conditions of the low-field NMR measurements.

Measurements	Variable	Fluid type	Nanoporous matrix	Number of fluid/solid ratio
T <sub>1</sub>	Pore diameter, temperature, fluid/solid ratio	H <sub>2</sub> O	Silica-4.0 nm; silica-2.5 nm; silica-1.5 nm	3
T <sub>2</sub>	Pore diameter, temperature, fluid/solid ratio	H <sub>2</sub> O	Silica-4.0 nm; silica-2.5 nm; silica-1.5 nm	3
T <sub>1</sub>	Pore diameter, temperature, fluid/solid ratio, fluid chemistry	CH <sub>3</sub> OH; H <sub>2</sub> O	Silica-4.0 nm	2
T <sub>2</sub>	Pore diameter, temperature, fluid/solid ratio, fluid chemistry	CH <sub>3</sub> OH; CH <sub>3</sub> OD	Silica-4.0 nm	3
T <sub>1</sub> , T <sub>2</sub>	Soaking time into water, temperature	H <sub>2</sub> O	Nanoporous silica rod-6.0 nm	2
Measurements	Fluid/solid ratio	Temperature (K) (H <sub>2</sub> O)	Temperature (K) (CH <sub>3</sub> OH/CD <sub>3</sub> OD)	Figures
T <sub>1</sub>	0.80 ml; 0.60 ml; 0.40 ml/0.150 g	298; 313; 323	-	2 (A-C)
T <sub>2</sub>	0.80 ml; 0.60 ml; 0.40 ml/0.150 g	298; 313; 323	-	3 (A-C)
T <sub>1</sub> , T <sub>2</sub>	0.60 ml; 0.40 ml/0.150 g	298; 313; 323	298; 313; 323	4 (A,B)
T <sub>1</sub> , T <sub>2</sub>	0.90 ml; 0.60 ml; 0.40 ml/0.150 g	-	298; 313; 323	5 (A,B)
T <sub>1</sub> , T <sub>2</sub>	10 and 90 min water soaking time	298; 313; 323	-	6 (A,B)

**TABLE 2** | T<sub>1</sub> and T<sub>2</sub> values of confined water obtained by keeping pore volumes approximately constant.

	Silica-4.0 nm	Silica-2.5 nm	Silica-1.5 nm
Amount (mg)	218.0	100.0	173.0
Total surface of given amount (m <sup>2</sup> )	130.1	116.7	143.9
Pore volume (cm <sup>3</sup> /g), single point at P/P <sub>0</sub> = 0.99	1.04	0.97	1.20
Pore volume for given amount of surface area (cm <sup>3</sup> )	125.1	120.3	119.9
T <sub>1</sub> (1) (ms)	500 ± 80	2,850 ± 60	2,670 ± 10
T <sub>1</sub> (2) (ms)	270 ± 50	-	-
T <sub>2</sub> (1) (ms)	19.6 ± 0.2	23.2 ± 0.4	18.5 ± 0.1
T <sub>2</sub> (2) (ms)	-	70.0 ± 2.0	-

The measurements were conducted at 313 K.

achieved using N<sub>2</sub> flow and BVT temperature control unit. T<sub>1</sub> measurements were completed using the inversion recovery pulse sequence found in the pulse sequence library of Bruker. T<sub>2</sub> relaxation measurements were performed utilizing the standard Carr-Pucell-Meiboom-Gill (CPMG) pulse sequence, with  $\tau$  of 1.0 ms between the 90 and 180° pulses. A continuous distribution of T<sub>2</sub> exponential decays and T<sub>1</sub> exponential growths correlated to confined and excess fluids were fitted for all T<sub>2</sub> and T<sub>1</sub> data using the CONTIN algorithm (Provencher, 1982). This analysis results in T<sub>2</sub> and T<sub>1</sub> distribution data. Bi-exponential decay and growth fittings of T<sub>2</sub> and T<sub>1</sub> curves, respectively, were completed using Origin 9.1 employing the following equations:

$$y = A_{21}e^{-x/T_{21}} + A_{22}e^{-x/T_{22}} \quad (1)$$

$$y = A_{21}e^{x/T_{11}} + A_{22}e^{x/T_{12}} \quad (2)$$

where T<sub>21</sub>, T<sub>22</sub>, T<sub>11</sub>, and T<sub>12</sub> are the relaxation constituents, and A<sub>21</sub> and A<sub>22</sub> are the corresponding scales. The amplitudes A<sub>21</sub> and A<sub>22</sub> are directly proportional to the amount of fluid either in confined state or as excess. The fraction of T<sub>21</sub> or T<sub>11</sub>

component is calculated as A<sub>21</sub>/(A<sub>21</sub>+A<sub>22</sub>) while portion of T<sub>22</sub> or T<sub>12</sub> component is determined as A<sub>22</sub>/(A<sub>21</sub>+A<sub>22</sub>).

## RESULTS AND DISCUSSION

### Characterization of the Nanoporous Silica Materials

**Figure S1** integrates the N<sub>2</sub> adsorption and desorption isotherms for the three samples. Based on the shapes of the isotherms, the 2.5 and 4.0 nm samples can be classified as *Type IV* (Sing et al., 1985), which possesses mesoporous structure and poses the hysteresis loop caused by capillary condensation in mesopores (Thommes et al., 2015). The silica-2.5 nm material does not show strong hysteresis character because it is near the boundary of mesopore and micropore size ranges. The silica-1.5 nm isotherm is complicated by a *Type I* isotherm (micropore) below 0.8 P/P<sub>0</sub>, and a mesoporous hysteresis loop above 0.8 P/P<sub>0</sub>. The hysteresis is like the *HI* type (Tangestaninejad et al., 2009), which is composed of regular pores that have narrow pore distribution. The insets in **Figure S1** show the pore size distributions for the three materials, where we can see that the silica-4.0 nm

and silica-2.5 nm have uniform pore sizes, as determined by the Barrett-Joyner-Halenda (BJH) desorption and adsorption models, respectively. On the other hand, the silica-1.5 nm shows a bimodal pore distribution, as determined by density functional theory (DFT) model, where the dominant pore sizes are  $\sim 1.5$  and  $\sim 2.5$  nm (see **Figure S1**-inset).

**Table S1** lists surface areas, volumes, and sizes of nanopores for the silica materials characterized for use in experiments. It needs to be mentioned that *meso*, which means “in between” in Greek, describes pore sizes ranging from 2.0 to 50.0 nm (Al-Othman, 2012; Thommes et al., 2015). In the present study, one of the silica samples, silica-1.5 nm, is out of the necessary range to be defined as *mesoporous*. This 1.5 nm material has higher surface area than the 4.0 nm material, contributed by the existence of micropores. In addition, the 2.5 nm material has relatively low pore volume, but the highest surface area measured, due to its nearly-microporous nature, and the highest surface-to-volume (S/V) ratio of the three porous silica systems. We will use the S/V ratio as a parameter for comparison in the discussion below.

**Figure S2** shows TXRD scans for the three samples, with the contribution from kapton foil removed. The three peaks of silica-4.0 nm, shown in **Figure S2a**, can be indexed as (100), (110), and (200) reflections, respectively (Sarawade et al., 2013). A hexagonal mesostructure with an interplanar distance of 4.5 nm [ $d_{(100)}$ ] can be determined, and based on the hexagonal geometry, the sum of the pore wall and pore diameter is about 5.2 nm. This long range ordered structure is consistent with the single peak ( $\sim 4.2$  nm) in the pore size distribution plot (**Figure S1**) determined from gas sorption analysis. In addition, the TEM imaging of this nanoporous silica shows an ordered arrangement of about 4.0 nm pores in parallel (Ok et al., 2017).

**Figure S2b** shows the five diffraction maxima observed in the TXRD scan of silica-2.5 nm, with  $d$ -spacings 3.1, 2.1, 1.9, 1.5, and 1.3 nm, respectively. According to their ratios, they can be indexed as (110), (200), (211), (310), and (222) reflections, and this ordered structure belongs to the cubic  $Im\bar{3}m$  space group. Therefore, the sum of the pore wall and the pore diameter is  $\sim 4.2$  nm, indicating that the pore wall is relatively thick, considering the pore diameter of 2.8 nm as determined by the BJH adsorption model. **Figure S2c** shows the silica-1.5 nm TXRD scan with diffraction maxima corresponding to  $d$ -spacings 2.2 and 1.5 nm. Although the specific pore structure arrangement is not identified in this case, these measurements, along with the pore distribution plot for silica-1.5 nm (**Figure S1**), suggest that it may have two dominant pore dimensions.

Pore volume is directly related to the amount of confined fluid. As demonstrated in **Figure S3a**, all of the porous silica samples where water was confined showed one-step mass loss. However, the samples with shorter drying times had fractions of water that persist till higher temperatures such as 200°C, as shown in **Figure S3a**, demonstrating representative weight loss in the case of silica-4.0 nm. As the sample-drying time was increased, complete weight-loss temperature shifted toward 95°C. In other words, all the water weight loss only required heating 95°C when the sample was dried for longer period of time. Similar results were observed when water was confined into silica samples with 2.5 and 1.5 nm pore diameters. At temperatures higher than

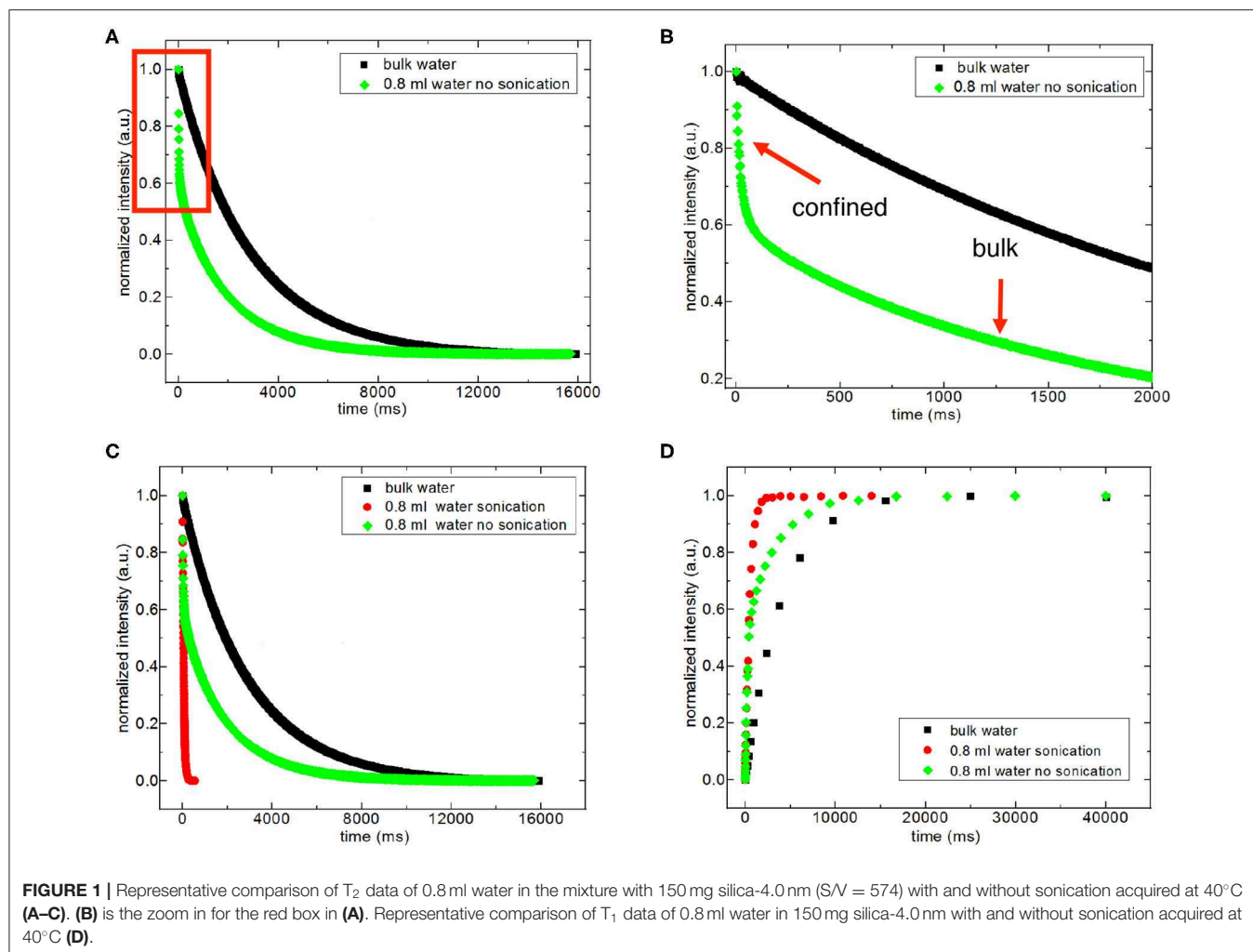
200°C no weight-loss occurred, and this shows that mesopores may intensely restrict water molecules and offer media for both thermodynamic and kinetic barrier to the elimination of water molecules (Wu and Navrotsky, 2013). These effects may resemble the consequences of confinement in geological environments with widely-ranging pore sizes. As shown in **Figure S3b**, the weight loss of water was less in silica-2.5 nm than for both silica-4.0 nm and silica-1.5 nm at the end of 12 min of drying time. This clearly showed that silica-2.5 nm has lower pore volume than the other two-engineered proxies of interest. Comparing the mass loss at the end of 20 min drying, we suggest that silica-1.5 nm has higher volume than that of silica-4.0 nm.

## Excess Fluid vs. Confined Fluid

For discriminating excess water signal from signal of water confined into nanoporous silica samples, first  $T_1$  (inversion recovery) and  $T_2$  (CPMG) measurements at 40°C on the low-field NMR instrument were conducted. **Figure S4a** shows excess water showing bulk-like behavior on top of the mixture of silica-4.0 nm and confined water. As seen in **Figure 1** and **Table 3A**, it is possible to differentiate excess water signal from that of confined water.  $T_1$  time values of bulk like water on top of the mixture without sonication are closer to that of water in bulk, while  $T_1$  values of confined water signal is lower than that of  $T_1$  values of confined water in the case of homogenized sample by sonication. This also exhibits that  $T_1$  values measured by homogenizing (sonication) are average values of water with two different environments: in between the grains and in the mesopores. Buntkowsky et al. (2007) mentioned that the sticking together is mainly the consequence of  $H_2O$  molecules high polarity and their capability to establish hydrogen bond networks among the water molecules. However, dynamics of water become more complicated in confined geometries due to opposition between the surface-liquid and liquid-liquid relations. This opposition forms new structures of water as in the case of partial ordering water molecules in the neighborhood of the restraining surface.

The other approach of the  $T_2$  data analysis belonging to the samples without sonication and with excess water on top (see **Figures S4a,d**) is determination of the percentages of bulk like water and confined water based on the Equation (1) as suggested in the literature (Aursand et al., 2008). This is a simple and robust technique to evaluate the  $T_2$  relaxation data. At first we compare the results of bi-exponential fitting of the data belonging to water mixtures with either silica-4.0 nm or silica-1.5 nm having bulk-like water on top as shown in **Figures S4a,d**. As seen in **Table 3A**, longer  $T_2$  values are assigned to bulk-like water. The percentage of bulk-like water on top of the mixture is not  $\sim <60\%$  (**Table 3B**). Then in this case, nearly 40% of  $H_2O$  is in between grains and confined establishing a dynamic system. Referring to **Table S1**, it is possible to calculate the pore volume given that the mass of the nanoporous silica is known. Thus, we can differentiate the volume of confined water from the volume of water in between the grains.

In the case of homogenized samples by sonication, because the nanoporous silica materials of interest in the current study have the same structure of MCM-41, we refer to the proposed filling mechanism of MCM-41 having 4.6 nm of pore-to-pore



distance by water (Grünberg et al., 2004). Water was studied as a guest molecule in mesoporous silica, MCM-41 and SBA-15, with two-dimensional hexagonally arranged of cylindrical pores in identical size ranging from 2 to 10 nm. Due to the high density of pores and relatively small pore diameters, these silica materials have bigger inner surfaces with respect to the volume of the single particle. There is a favored axis present in the direction of the pores cylinder axis arising from highly anisotropic geometry of the pores. In MCM-41, following the first wetting of the pore surfaces, a co-presence of filled pores or partially filled pores occurs. Additional filling of the pores happens as an enlargement of the filled pores till whole filling is obtained once more. Therefore, for MCM-41 the water layer grows axially in the direction of the pore axis. In the case of 0.4 ml  $H_2O$  wetted silica-4.0 nm or silica-1.5 nm there were initially wetted pore surfaces, filled pores and not wetted pore (dry) segments coexisted. In mixtures of nanoporous silica samples mixed with either 0.6 or 0.8 ml  $H_2O$ , after homogenization by 15 min sonication, the confined water molecules were in rapid “conversation” with the excess water molecules occupying the space in between the grains. The water molecules inside the

nanoporous silica did the fast exchange with the excess water molecules by moving axially in the direction of the pores. On the NMR time scale, average  $T_1$  or  $T_2$  values were obtained. These average relaxation times are shorter than not only these of bulk water but also bulk-like water on top of the silica and water mixtures. There was no apparent bulk-like water in the case of mixtures with 0.4 ml water. For this reason, we did not apply bi-exponential fitting analysis for these samples having the lowest fluid-to-solid ratio.

### Dynamics of Confined Fluids

Then we focus on dynamical behaviors of confined fluids by varying temperature, fluid-to-solid ratio, and pore diameter. **Table 4A** lists  $T_1$  values of bulk and confined water. As seen in **Figures 2A–C**, deviation and change of confined fluid behavior from that of bulk fluid is independent of pore size of the nanoporous matrix systems. At the fluid-to-solid ratios of 0.8, 0.6, and 0.4 ml to 150 mg silica-2.5 nm,  $T_1$  times increased as the temperature was increased. However, in the case of fluid-to-solid ratios of 0.8, 0.6, and 0.4 ml to 150 mg silica-4.0 nm,  $T_1$  times did not show significant change when temperature

**TABLE 3A** |  $T_1$  and  $T_2$  values of confined water measured on the 20 MHz instrument at 40°C with either excess water on top or after homogenization with sonication.

Sample	$T_2$ (ms)	$T_1$ (ms)	Experimental treatment
Bulk water	2,883.3 ± 0.5	3,960 ± 20	-
150 mg silica-4.0 nm + 0.8 ml H <sub>2</sub> O	(1): 50.48 ± 0.08	(1): 478 ± 6	After sonication
150 mg silica-4.0 nm + 0.8 ml H <sub>2</sub> O	(1): 34.5 ± 0.2	<b>(1): 200 ± 8</b>	Without sonication/with excess fluid
	(2): 1,956 ± 1	<b>(2): 3,300 ± 100</b>	
150 mg silica-4.0 nm + 0.6 ml H <sub>2</sub> O	(1): 36.48 ± 0.06	(1): 350 ± 10	After sonication
		(2): 470 ± 20	
150 mg silica-4.0 nm + 0.6 ml H <sub>2</sub> O	(1): 29.4 ± 0.1	<b>(1): 201 ± 87</b>	Without sonication/with excess fluid
	(2): 2,315 ± 1	<b>(2): 3,500 ± 100</b>	
150 mg silica-2.5 nm + 0.8 ml H <sub>2</sub> O	(1): 24.2 ± 0.3	(1): 2,830 ± 20	After sonication
	(2): 91.0 ± 3.0		
150 mg silica-2.5 nm + 0.8 ml H <sub>2</sub> O	(1): 15 ± 2.0	(1): 2,760 ± 20	Without sonication/with excess fluid
	(2): 38.6 ± 0.7		
150 mg silica-2.5 nm + 0.6 ml H <sub>2</sub> O	(1): 17.0 ± 5.0	(1): 2,660 ± 20	After sonication
150 mg silica-2.5 nm + 0.6 ml H <sub>2</sub> O	(1): 17.57 ± 0.10	(1): 70 ± 20	Without sonication/with excess fluid
		(2): 2,600 ± 10	
150 mg silica-1.5 nm + 0.8 ml H <sub>2</sub> O	(1): 9.6 ± 0.2	(1): 2,200 ± 200	After sonication
	(2): 55.1 ± 0.6	(2): 1,100 ± 200	
150 mg silica-1.5 nm + 0.8 ml H <sub>2</sub> O	(1): 5.74 ± 0.03	<b>(1): 110 ± 2</b>	Without sonication/with excess fluid
	(2): 1,406.9 ± 0.4	<b>(2): 2,800 ± 100</b>	
150 mg silica-1.5 nm + 0.6 ml H <sub>2</sub> O	(1): 5.1 ± 0.5	(1): 1,000 ± 50	After sonication
	(2): 41.7 ± 0.1	(2): 2,100 ± 100	
150 mg silica-1.5 nm + 0.6 ml H <sub>2</sub> O	(1): 16.7 ± 0.10	<b>(1): 680 ± 20</b>	Without sonication/with excess fluid
	(2): 927.1 ± 0.6	<b>(2): 3,500 ± 10</b>	

*Bold and italic values are with excess fluid on top. In particular,  $T_1(2)$  are the values closer to that of bulk fluid.*

**TABLE 3B** | Quantification of confined vs. excess water.

Sample	Treatment	$A_{21}$ (longer $T_2$ )	$A_{22}$ (shorter $T_2$ )	Amount of H <sub>2</sub> O on top (ml)	The rest of H <sub>2</sub> O (ml) <sup>a</sup>	Amount of H <sub>2</sub> O between grains (ml) <sup>b</sup>	Confined H <sub>2</sub> O (ml) <sup>c</sup>	Pore volume (ml) <sup>d</sup>
150 mg silica-4.0 nm + 0.8 ml H <sub>2</sub> O	Centrifuge/with excess fluid	0.61	0.39	0.49	0.31	0.16	0.16	0.16
150 mg silica-4.0 nm + 0.6 ml H <sub>2</sub> O	Centrifuge/with excess fluid	0.63	0.38	0.38	0.23	0.07	0.16	0.16
150 mg silica-1.5 nm + 0.8 ml H <sub>2</sub> O	Centrifuge/with excess fluid	0.53	0.47	0.42	0.38	0.20	0.18	0.18
150 mg silica-1.5 nm + 0.6 ml H <sub>2</sub> O	Centrifuge/with excess fluid	0.60	0.40	0.36	0.24	0.06	0.18	0.18

<sup>a</sup>Volume of water confined and between grains.

<sup>b</sup>Difference between 1 and 3.

<sup>c</sup>Volume of confined water which is equal to pore volume.

<sup>d</sup>Pore volume determined by using density data in **Table S1**.

was varied. When 0.8 ml water was confined to 150 mg silica-1.5 nm, as the temperature was increased,  $T_1$  times also increased. However, with the fluid-to-solid ratios of 0.6 and 0.4 ml water to 150 mg silica-1.5 nm, first there was an increase in  $T_1$  time as the temperature was increased, but when the temperature was increased further,  $T_1$  time decreased. Sattig et al. (2014) studied temperature-dependent rotational motion of super-cooled H<sub>2</sub>O in MCM-41 type silica pores of diameters 2.93, 2.76, and 2.14 nm using <sup>2</sup>H NMR. There was a first sharp twist observed in the temperature reliance escorted by a solidification of a portion of the confined H<sub>2</sub>O. This implied an alteration from bulk-like to interface-dominated water dynamics instead of a

liquid-liquid phase changeover. In the temperature range above 225 K, there was the confinement effect observed. Above 225 K, the temperature reliance of H<sub>2</sub>O re-location was weaker in the smaller pores, and in the bigger pores bulk-like water behavior was seen. Near 225 K, longitudinal magnetization relaxation ( $T_1$ ) times for the ice in silica-2.1 nm confinement became very long for a dependable determination within a sensible duration, while  $T_1$  times for confined water in liquid state passes a minimum, showing that confined H<sub>2</sub>O has correlation times  $\tau \approx 1/\omega_0 \approx 1$  ns. It was suggested that <sup>2</sup>H NMR line-shape analysis evidenced pronounced dynamical heterogeneities for confined H<sub>2</sub>O. However, in our study we did not conduct line-shape

**TABLE 4A** | Longitudinal magnetization relaxation times ( $T_1$ ) of confined water obtained after sonication of the mixtures for 15 min.

Samples	Temperature (°C)		
	25°C	40°C	50°C
Bulk H <sub>2</sub> O	2,960 ± 20 ms	3,960 ± 20 ms	4,440 ± 50 ms
150 mg silica-4.0 nm + 0.8 ml H <sub>2</sub> O	(1): 413 ± 30 ms	(1): 478 ± 6 ms	(1): 550 ± 10 ms
150 mg silica-4.0 nm + 0.6 ml H <sub>2</sub> O	(1): 270 ± 8 ms (2): 360 ± 10 ms	(1): 350 ± 10 ms (2): 470 ± 20 ms	(1): 405 ± 3 ms
150 mg silica-4.0 nm + 0.4 ml H <sub>2</sub> O	(1): 210 ± 20 ms (2): 310 ± 30 ms	(1): 254 ± 9 ms (2): 400 ± 10 ms	(1): 30 ± 6 ms (2): 329 ± 5 ms
150 mg silica-2.5 nm + 0.8 ml H <sub>2</sub> O	(1): 2,230 ± 20 ms	(1): 2,830 ± 20 ms	(1): 3,510 ± 80 ms
150 mg silica-2.5 nm + 0.6 ml H <sub>2</sub> O	(1): 2,120 ± 20 ms	(1): 2,660 ± 20 ms	(1): 3,120 ± 20 ms
150 mg silica-2.5 nm + 0.4 ml H <sub>2</sub> O	(1): 1,970 ± 60 ms	(1): 2,370 ± 10 ms	(1): 2,720 ± 30 ms
150 mg silica-1.5 nm + 0.8 ml H <sub>2</sub> O	(1): 1,000 ± 200 ms (2): 1,800 ± 300 ms	(1): 1,100 ± 200 ms (2): 2,200 ± 200 ms	(1): 1,390 ± 70 ms (2): 3,100 ± 300 ms
150 mg silica-1.5 nm + 0.6 ml H <sub>2</sub> O	(1): 900 ± 100 ms (2): 1,700 ± 400 ms	(1): 1,000 ± 50 ms (2): 2,100 ± 100 ms	(1): 700 ± 200 ms (2): 2,200 ± 400 ms
150 mg silica-1.5 nm + 0.4 ml H <sub>2</sub> O	(1): 670 ± 100 ms (2): 800 ± 100 ms	(1): 500 ± 100 ms (2): 1,440 ± 40 ms	(1): 130 ± 40 ms (2): 1,060 ± 10 ms

analysis; rather focus on  $T_1$  measurements at high temperatures. Temperature range of the study was out of interest of the current contribution. However, Sattig et al. (2014) mentioned that the temperature reliance of water re-location is largely independent of the confinement dimensions. We observe a similar result that deviation of confined water behavior from that of bulk water is independent of pore diameter, while degree of confinement effect on dynamics of confined water is more pronounced in the case of silica-4.0 nm. This is reflected in the  $T_1$  values as follows: the longest  $T_1$  values were observed when water was confined to silica-2.5 nm, while the shortest  $T_1$  values were seen when water was confined to silica-4.0 nm. We explain this situation with surface-to-volume ( $S/V$ ) ratios of the nanoporous silica materials rather than pore diameter. Timur (1969) claimed that in a three-component NMR model, the pore volumes of a porous medium were classified as three sub-groups, based on their  $S/V$  ratio distribution. He explained that the longer  $T_1$  times would correspond to the smaller  $S/V$  ratios, and the larger pores. In our case, the  $T_1$  times do not show systematic change as a function of pore diameter. Rather,  $T_1$  times become longer when water molecules are confined into silica-2.5 nm with the highest  $S/V$  ratio, while the shortest  $T_1$  times are observed upon confining H<sub>2</sub>O molecules into silica-4.0 nm with the lowest  $S/V$  ratio. For this reason, the trend in  $T_1$  times of water confined into silica materials is attributed to the  $S/V$  ratios rather than pore diameter.

Besides analyzing  $T_1$  times,  $T_2$  times of the confined fluids were also analyzed. **Table 4B** lists the  $T_2$  results. As seen in **Figures 3A–C**, when the fluid-to-solid ratio is decreased,  $T_2$  values also decrease. This is independent of the pore diameter of the nanoporous silica materials.  $T_2$  values in the case of the fluid-to-solid ratio of 0.4 ml to 150 mg silica (partial filling of the pores) are longer for silica-4.0 nm than silica-1.5 nm and silica-2.5 nm. In the case of 0.6 ml fluid to 150 mg silica ratio,  $T_2$  values of water confined into silica-4.0 nm and silica-1.5 nm

are closer to each other, and longer than confined into silica-2.5 nm. With the highest fluid-to-solid ratio, the longest  $T_2$  values are observed when water is confined into silica-2.5 nm. Having smaller fluid-to-solid ratio means filling the pores with lower volume easily. Because silica-2.5 nm has lower pore volume as shown by TGA measurements (see **Figures S3a,b**), in the case of the lowest fluid-to-solid ratio “majority” of the fluid molecules completely fill the pores. This in turn is indicated with shorter  $T_2$  values. There is an important trend in  $T_2$  values. As the fluid-to-solid ratio is decreased,  $T_2$  values also decrease. However, the decrease is more effective in the case of silica-2.5 nm, which has the lowest pore volume.

The other set of measurements was conducted by keeping the pore volume of each nanoporous silica constant around 120 cm<sup>3</sup> (see **Table 2**). Among the three silica samples, silica-2.5 nm has the highest  $S/V$  ratio. When the pore volume is kept constant at ~120 cm<sup>3</sup>, water has the longest  $T_1$  value in the mixture with silica-2.5 nm. Similarly, the highest  $T_2$  was obtained for the same water and silica-2.5 nm mixture. The  $T_1$  value of water in the mixture with silica-1.5 nm is slightly lower than that of water in the mixture with silica-2.5 nm. The results on relaxation of water obtained by keeping pore volumes of porous matrixes constant for the given amounts of the porous materials indicate clearly that pore diameter does not affect the dynamics of confined water significantly. Rather,  $S/V$  ratio along with pore diameter reflects information on filling mechanism of nanoporous silica materials with water. In particular, when the pore diameter is big and  $S/V$  ratio is small, at first water molecules wet the surface of the pore walls. Additional filling happens easily from the pore wall to the midpoint of the pore. Then complete filling of the pores is achieved (Grünberg et al., 2004). In the case of nanoporous silica with small pore diameter and large  $S/V$  ratio, the filling mechanism occurs in a different way: first the center is filled; hence there is a co-presence of filled pore fragments with wetted pores. Further filling of the pores develops axially in the direction

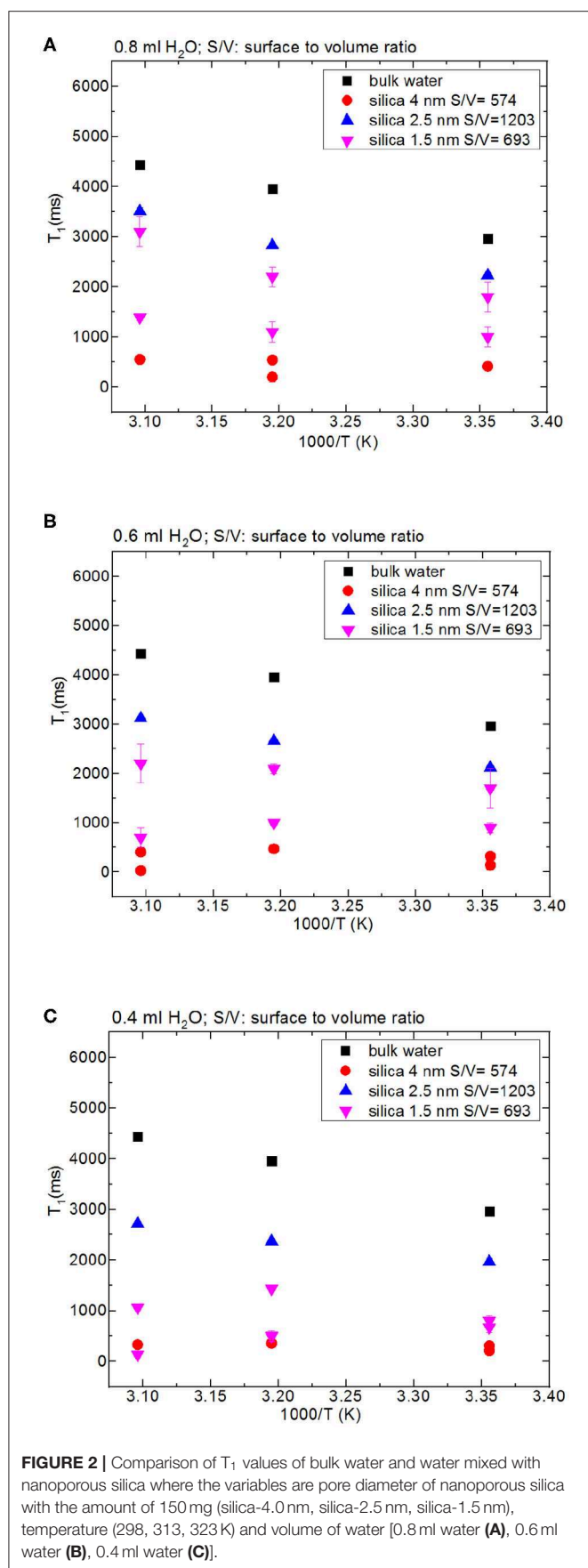


**FIGURE 2** | Comparison of  $T_1$  values of bulk water and water mixed with nanoporous silica where the variables are pore diameter of nanoporous silica with the amount of 150 mg (silica-4.0 nm, silica-2.5 nm, silica-1.5 nm), temperature (298, 313, 323 K) and volume of water [0.8 ml water (A), 0.6 ml water (B), 0.4 ml water (C)].

of the pore axis. The pore volume is also related to pore length when we assume cylindrical pores. The nanoporous silica with small pore diameter and long pore axis leads to larger pore volumes. The long pore length (large pore volume) gives enough degree of freedom for confined water molecules. Relatively free confined water molecules prefer motion in axial direction, and this results in weaker interactions with pore walls. This is a possible explanation of larger  $T_1$  values for pores with smaller pore diameter and larger pore volume.

In addition to the effect of pore volume and S/V ratios of the porous systems on dynamical behaviors of confined H<sub>2</sub>O, fluid chemistry is also studied by confining CH<sub>3</sub>OH and CH<sub>3</sub>OD into nanoporous silica-4.0 nm. **Tables 5A,B** list  $T_1$  and  $T_2$  values of bulk and confined CH<sub>3</sub>OH and CH<sub>3</sub>OD. First,  $T_1$  and  $T_2$  relaxation times of confined methanol deviated from those of bulk methanol. The second remarkable point is the higher  $T_1$  and  $T_2$  values of CH<sub>3</sub>OD with respect of those of CH<sub>3</sub>OH in confined state. Internal rotation of the -CH<sub>3</sub> group is faster than the -OD group rotation in turn leading to longer  $T_1$  times of CH<sub>3</sub>OD compared to that of CH<sub>3</sub>OH. As seen in **Figures 4A,B**, confined methanol (CH<sub>3</sub>OH) has slightly higher  $T_1$  relaxation values than these of confined H<sub>2</sub>O. This result is independent of fluid-to-solid ratio. This is also related to the faster internal rotation of -CH<sub>3</sub> group. As expected, when the fluid-to-solid ratio is decreased,  $T_1$  values of confined methanol also decreased. Methanol has two  $T_1$  values in confined state. In the case of higher fluid-to-solid ratio, longer  $T_1$  increases as temperature increases, while shorter  $T_1$  does not show significant change upon elevating temperature. In the case of lower fluid-to-solid ratio for both longer and shorter  $T_1$  values,  $T_1$  minimum is observed as a function of temperature.

Methanol has also two  $T_2$  values in confined state (**Figures 5A,B**). The longer  $T_2$  value is greater than of that H<sub>2</sub>O. The longer  $T_2$  value increases as temperature increases, while the shorter  $T_2$  does not indicate significant change when temperature is varied. When the fluid-to-solid ratio was decreased,  $T_2$  values also decreased. The short  $T_2$  value of CH<sub>3</sub>OH in the confined state became even shorter as the temperature was elevated. This is independent of the fluid-to-solid ratios. This observation is explained by layering of CH<sub>3</sub>OH on the pore walls via interacting with -OH groups of the pores, which are proven to exist by solid-state magic angle spinning (MAS) cross-polarization (CP) NMR (Sindorf and Maciel, 1983). In addition, water molecules near the interface had preferred directions due to the interaction with surface -OH groups (Millischuk and Ladanyi, 2011). There are two layers, and as temperature was elevated the molecules of the second layer having weaker interactions with the molecules forming the first layer with -OH of the pore walls gained mobility, and moved to the region of the molecules clustered in the middle of the pores. The number of methanol molecules in the second layer was reduced when the temperature was increased, while methanol molecules of the first layer still interact with the pore walls. Thus, the shorter  $T_2$  value attributed to the average motions of the first and second layers of CH<sub>3</sub>OH interacting with the pore walls became shorter at high temperatures. However, there is weaker hydrogen bonding interaction between CH<sub>3</sub>OH and -OH of the pore walls that is indicated in relatively longer  $T_1$

**TABLE 4B** | Transverse magnetization relaxation times ( $T_2$ ) of confined water obtained after sonication of the mixtures for 15 min.

Samples	Temperature (°C)		
	25°C	40°C	50°C
Bulk H <sub>2</sub> O	2,440 ± 0.2	2,883.3 ± 0.5	3,122.2 ± 0.2
150 mg silica-4.0 nm + 0.8 ml H <sub>2</sub> O	(1): 47.0 ± 2.0 ms (2): 53.0 ± 2.0 ms	(1): 50.5 ± 0.1 ms	(1): 75.3 ± 0.1 ms
150 mg silica-4.0 nm + 0.6 ml H <sub>2</sub> O	(1): 37.6 ± 0.1 ms	(1): 36.5 ± 0.1 ms	(1): 58.8 ± 0.1 ms
150 mg silica-4.0 nm + 0.4 ml H <sub>2</sub> O	(1): 29.4 ± 0.2 ms (2): 6.1 ± 0.9 ms	(1): 27.8 ± 0.1 ms	(1): 44.3 ± 0.6 ms (2): 14.0 ± 2.0 ms
150 mg silica-2.5 nm + 0.8 ml H <sub>2</sub> O	(1): 27.2 ± 0.4 ms (2): 99.0 ± 4.0 ms	(1): 24.2 ± 0.3 ms (2): 91.0 ± 3.0 ms	(1): 27.5 ± 0.2 ms (2): 119 ± 4.0 ms
150 mg silica-2.5 nm + 0.6 ml H <sub>2</sub> O	(1): 19.7 ± 0.1 ms	(1): 17.0 ± 5.0 ms	(1): 19.3 ± 0.1 ms
150 mg silica-2.5 nm + 0.4 ml H <sub>2</sub> O	(1): 12.5 ± 0.1 ms	(1): 11.0 ± 0.1 ms (2): 24.3 ± 0.4 ms	(1): 12.8 ± 0.1 ms
150 mg silica-1.5 nm + 0.8 ml H <sub>2</sub> O	(1): 10.1 ± 0.5 ms (2): 42.8 ± 0.3 ms	(1): 9.6 ± 0.2 ms (2): 55.1 ± 0.6 ms	(1): 10.7 ± 0.2 ms (2): 62.2 ± 0.3 ms
150 mg silica-1.5 nm + 0.6 ml H <sub>2</sub> O	(1): 13.3 ± 1.0 ms (2): 44.4 ± 0.5 ms	(1): 5.1 ± 0.5 ms (2): 41.7 ± 0.1 ms	(1): 4.9 ± 0.5 ms (2): 43.3 ± 0.1 ms
150 mg silica-1.5 nm + 0.4 ml H <sub>2</sub> O	(1): 8.3 ± 0.5 ms (2): 21.3 ± 0.3 ms	(1): 7.4 ± 0.5 ms (2): 19.1 ± 0.3 ms	(1): 15.9 ± 0.1 ms

values of CH<sub>3</sub>OH with respect to these of H<sub>2</sub>O. As discussed above, the contribution of faster internal –CH<sub>3</sub> rotation to the overall dynamics of CH<sub>3</sub>OH molecules should not be neglected as well.

## Dynamics of Water Confined in Nanoporous Silica Monoliths Without Excess Fluid

First, it needs to be mentioned that there was no excess fluid in the medium when both of the  $T_1$  and  $T_2$  measurements were conducted upon soaking the nanoporous silica monoliths into water. The surface area of the nanoporous silica monolith is closer to that of silica-4.0 nm. **Table 6** lists  $T_1$  and  $T_2$  values of water confined in the nanoporous silica monolith by varying soaking duration and temperature (see **Figure 6**). In this case, 10 min and 90 min of soaking time correspond to partial filling and more complete saturation of water in pores, respectively. Both  $T_1$  and  $T_2$  times of confined water in the nanoporous silica monoliths show strong deviation from bulk values (see **Tables 4A,B**) for bulk  $T_1$  and  $T_2$  relaxation values of water, respectively). The deviation from bulk is independent of the water soaking time. Comparison of the  $T_1$  values water molecules inside the nanoporous silica monoliths shows the negligible effect of soaking duration. However,  $T_2$  times get shorter approximately twice as the soaking time was increased to 90 min. As expected, when the temperature was increased, both  $T_1$  and  $T_2$  times of confined water within the nanoporous silica monoliths get longer, and again independent of the soaking time. The shortest  $T_2$  value observed is explained by the strong interaction between the confined water molecules and the pore walls of the nanoporous silica monolith surface. We suggest that there is first a monolayer established on top of the pore walls of the monolith. This layer gains mobility when the temperature

was increased in the case of short soaking time. However, such a mobility and hence increase in the shorter  $T_2$  time component is not observed in the case of 90 min soaking time sample. In other words, partial filling of the pores due to shorter soaking time gives free volume within the nanoporous silica monolith for confined water molecules. The elevation in temperature helps with overcoming energy barrier that water molecules forming the monolayer gain freedom. This gain in mobility is reflected as longer relaxation times. In comparing the relaxation times of confined water in nanoporous silica monoliths with respect to the relaxation values of H<sub>2</sub>O confined into nanoporous powdered silica samples (silica-4.0 nm, silica-2.5 nm, and silica-1.5 nm), we prefer to consider the samples where only 0.4 ml water was confined into the powdered silica samples.  $T_1$  values of water within the nanoporous silica monoliths are significantly shorter than those of water confined into silica-2.5 nm and silica-1.5 nm, while closer but still shorter than that of water confined into silica-4.0 nm.  $T_2$  times of water confined into nanoporous silica monolith for 10 min of soaking time are longer than those of  $T_2$  times of water confined into powdered nanoporous silica samples, but  $T_2$  times of water confined into nanoporous silica monolith for 90 min of soaking time are within the same range with  $T_2$  values of water confined into powdered nanoporous silica matrixes. The comparison shows that confinement effect for water is independent of water soaking time. The water molecules remaining between powdered nanoporous silica grains upon sonication, where only 0.4 ml water was confined into the powdered silica samples, contribute to the averaged relaxation times so that relatively longer  $T_1$  and  $T_2$  times than those of water within the nanoporous silica monoliths were observed. There is an overall decreasing trend in relaxation times of water as going from smaller pore diameters of 1.5 and 2.5 nm to larger diameters of 4.0 and 6.0 nm. As a result, we suggest that taking the pore diameters of both the powdered and monolith samples into

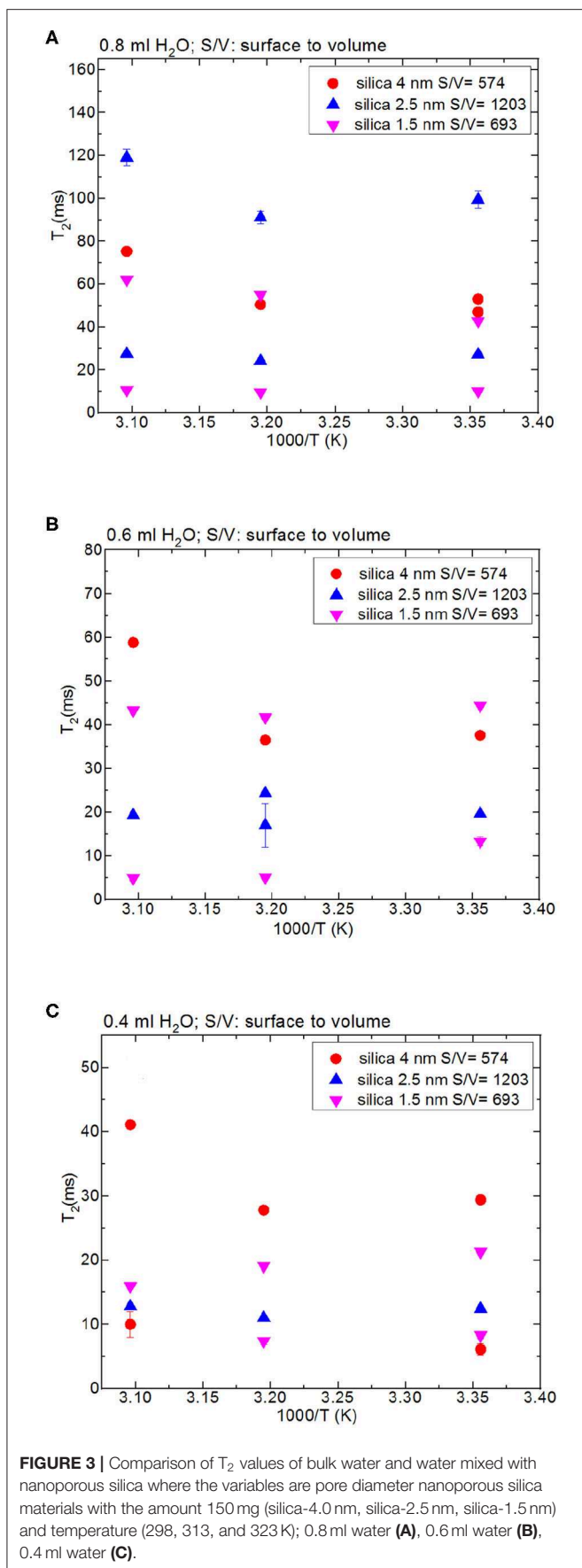


**FIGURE 3** | Comparison of  $T_2$  values of bulk water and water mixed with nanoporous silica where the variables are pore diameter nanoporous silica materials with the amount 150 mg (silica-4.0 nm, silica-2.5 nm, silica-1.5 nm) and temperature (298, 313, and 323 K); 0.8 ml water (A), 0.6 ml water (B), 0.4 ml water (C).

account, pore volume is a significant factor reducing the mobility of water.

### $T_1/T_2$ Ratio of Confined Fluid Interaction With the Pore Walls

Regarding NMR relaxation in porous media,  $T_1/T_2$  ratio indicates how strongly or weakly molecules interact with the uppermost layer of the porous system (Mitchell et al., 2009; Weber et al., 2009). Therefore,  $T_1/T_2$  ratio is an important parameter showing the degree of wettability of the fluid toward pore walls in confined geometry. The NMR  $T_1$  time in liquids arises from time-dependent local magnetic fields persuading changeovers that permit nuclear spins to restore the equilibrium. The major driving force for variations in local magnetic fields at a nucleus is the rotational motion of molecules, regularly defined as molecular tumbling. The correlation time of molecular tumbling is defined as  $\tau_c$ . The approximate definition of  $\tau_c$  is the duration for a molecule to finish a rotation of 1 rad. The BPP (Bloemberg-Purcell-Pound) relaxation theory describes that for  $\tau_c \rightarrow 0$ ,  $T_1 \rightarrow \infty$ . As a result, small, and rapid tumbling molecules will show a gradual relaxation rate and thus longer  $T_1$  values (Bloembergen et al., 1948; D'Agostino et al., 2012). There is the resulting correlation between  $T_1$  and  $\tau_c$ :

$$\frac{1}{T_1} \propto \frac{\tau_c}{1 + (2\omega_0\tau_c)^2} \quad (3)$$

where  $\omega_0$  is the precession frequency of the target nucleus. This equation tells that for very fast molecular motion (when  $1/\tau_c \gg 2\omega_0$ ),  $T_1$  is inversely proportional to  $\tau_c$ . That is, as correlation time decreases (fast molecular motion), relaxation time increases (the rate of relaxation decreases). Conversely, for slow molecular motion (when  $1/\tau_c \ll 2\omega_0$ ),  $T_1$  is directly proportional to  $\tau_c$ . Therefore, they both increase together. The minimum in  $T_1$ , and hence the most efficient spin-lattice relaxation, occurs when  $\tau_c \propto (\omega_0)^{-1}$  (Slichter, 1990; Macomber, 1998; Nicotera et al., 2012). Viscous molecules or molecules under confinement of geometrical constraints will have shorter  $T_1$  values and thus a faster relaxation rate (D'Agostino et al., 2012). In analyzing and explaining the longitudinal relaxation data obtained, we refer to Equation (4) described below. We first think of a cylindrical pore with a radius of  $R$  and a length of  $l$ , completely filled with water molecules. Due to water-substrate interactions, the water molecules at the surface will experience a restricted motion when compared to the bulk like water in the middle of pore. We assume that the water molecules within a distance  $a$  from the surface are affected by the surface and the rest acts as bulk like fluid as mentioned above while discussing layering of methanol on the pore walls via interactions with  $-OH$  groups decorating the pore walls. Under these assumptions the observed proton relaxation time constant  $T_{1,observed}$  will have a weighted average from water molecules near the surface and bulk like water molecules, where the weights are proportional to the volume (Gallegos et al., 1988; Weber et al., 2009). The number of protons/water molecules at the uppermost layer and in bulk-like state is proportional to the  $V_{Surface}$  and  $V_{Bulk}$ , respectively. Thus, the observed  $T_{1,observed}$

**TABLE 5A** | Longitudinal magnetization relaxation times ( $T_1$ ) of confined  $\text{CH}_3\text{OH}$  and  $\text{CH}_3\text{OD}$  obtained after sonication of the mixtures for 15 min.

Samples	Temperature ( $^{\circ}\text{C}$ )		
	25 $^{\circ}\text{C}$	40 $^{\circ}\text{C}$	50 $^{\circ}\text{C}$
<b>Bulk <math>\text{CH}_3\text{OH}</math></b>	<b>2,800 <math>\pm</math> 20 ms</b>	<b>3,300 <math>\pm</math> 100 ms</b>	<b>3,320 <math>\pm</math> 20</b>
150 mg silica-4.0 nm + 0.9 ml $\text{CH}_3\text{OH}$	(1): 50 $\pm$ 30 ms (2): 540 $\pm$ 10 ms	(1): 200 $\pm$ 40 ms (2): 670 $\pm$ 20 ms	(1): 520 $\pm$ 70 ms (2): 900 $\pm$ 100 ms
150 mg silica-4.0 nm + 0.6 ml $\text{CH}_3\text{OH}$	(1): 100 $\pm$ 10 ms (2): 465 $\pm$ 6 ms	(1): 100 $\pm$ 30 ms (2): 530 $\pm$ 10 ms	(1): 150 $\pm$ 20 ms (2): 630 $\pm$ 30 ms
150 mg silica-4.0 nm + 0.4 ml $\text{CH}_3\text{OH}$	(1): 120 $\pm$ 20 ms (2): 400 $\pm$ 21 ms	(1): 40 $\pm$ 20 ms (2): 390 $\pm$ 10 ms	(1): 140 $\pm$ 30 ms (2): 470 $\pm$ 20 ms
<b>Bulk <math>\text{CH}_3\text{OD}</math></b>	<b>2,790 <math>\pm</math> 30 ms</b>	<b>3,170 <math>\pm</math> 50 ms</b>	<b>3,280 <math>\pm</math> 40 ms</b>
150 mg silica-4.0 nm + 0.9 ml $\text{CH}_3\text{OD}$	(1): 1,290 $\pm$ 10 ms	(1): 1,560 $\pm$ 30 ms	(1): 1,300 $\pm$ 200 ms (2): 2,000 $\pm$ 200 ms
150 mg silica-4.0 nm + 0.6 ml $\text{CH}_3\text{OD}$	(1): 100 $\pm$ 20 ms (2): 670 $\pm$ 6 ms	(1): 780 $\pm$ 20 ms	(1): 680 $\pm$ 80 ms (2): 1,000 $\pm$ 100 ms
150 mg silica-4.0 nm + 0.4 ml $\text{CH}_3\text{OD}$	(1): 390 $\pm$ 40 ms (2): 630 $\pm$ 60 ms	(1): 580 $\pm$ 20 ms	(1): 650 $\pm$ 20 ms

**TABLE 5B** | Transverse magnetization relaxation times ( $T_2$ ) of confined  $\text{CH}_3\text{OH}$  obtained after sonication of the mixtures for 15 min.

Samples	Temperature ( $^{\circ}\text{C}$ )		
	25 $^{\circ}\text{C}$	40 $^{\circ}\text{C}$	50 $^{\circ}\text{C}$
Bulk $\text{CH}_3\text{OH}$	2,589.5 $\pm$ 0.1 ms	2,780.9 $\pm$ 0.2 ms	2,985.6 $\pm$ 0.2 ms
150 mg silica-4.0 nm + 0.9 ml $\text{CH}_3\text{OH}$	(1): 59.1 $\pm$ 0.8 ms (2): 338.5 $\pm$ 0.4 ms	(1): 61.9 $\pm$ 0.6 ms (2): 396.1 $\pm$ 0.3 ms	(1): 53.0 $\pm$ 0.3 ms (2): 434.5 $\pm$ 0.3 ms
150 mg silica-4.0 nm + 0.6 ml $\text{CH}_3\text{OH}$	(1): 49.9 $\pm$ 0.5 ms (2): 307.3 $\pm$ 0.4 ms	(1): 44.2 $\pm$ 0.5 ms (2): 327.1 $\pm$ 0.4 ms	(1): 39.1 $\pm$ 0.3 ms (2): 386.2 $\pm$ 0.3 ms
150 mg silica-4.0 nm + 0.4 ml $\text{CH}_3\text{OH}$	(1): 32.1 $\pm$ 0.4 ms (2): 171.3 $\pm$ 0.4 ms	(1): 28.2 $\pm$ 0.3 ms (2): 196.1 $\pm$ 0.3 ms	(1): 23.2 $\pm$ 0.2 ms (2): 209.8 $\pm$ 0.3 ms
Bulk $\text{CH}_3\text{OD}$	2,588.6 $\pm$ 0.2 ms	2,790.3 $\pm$ 0.4 ms	2,937.3 $\pm$ 0.2 ms
150 mg silica-4.0 nm + 0.9 ml $\text{CH}_3\text{OD}$	(1): 58 $\pm$ 2 ms (2): 636.1 $\pm$ 0.3 ms	(1): 64 $\pm$ 2 ms (2): 732.8 $\pm$ 0.3 ms	(1): 38 $\pm$ 1 ms (2): 807.2 $\pm$ 0.2 ms
150 mg silica-4.0 nm + 0.6 ml $\text{CH}_3\text{OD}$	(1): 48 $\pm$ 1 ms (2): 422.0 $\pm$ 0.3 ms	(1): 145 $\pm$ 3 ms (2): 521.5 $\pm$ 0.8 ms	(1): 32.7 $\pm$ 1.0 ms (2): 527.5 $\pm$ 0.2 ms
150 mg silica-4.0 nm + 0.4 ml $\text{CH}_3\text{OD}$	(1): 58 $\pm$ 2 ms (2): 231.9 $\pm$ 0.6 ms	(1): 59 $\pm$ 3 ms (2): 259.2 $\pm$ 0.8 ms	(1): 50 $\pm$ 2 ms (2): 273.4 $\pm$ 0.5 ms

relaxation can be written as:

$$\frac{1}{T_{1,observed}} = \frac{2a}{R} \left[ \frac{1}{T_{1,surface}} - \frac{1}{T_{1,bulk}} \right] + \left[ \frac{1}{T_{1,bulk}} \right] \quad (4)$$

This equation assumes an ideal case where the pores are filled in whole with the liquid of interest. In the current study, there is gradual increase in the amount of fluid mixed with the porous systems. This leads to an increase in the amount of confined fluid. **Tables 7A,B** lists the  $T_{1,surface}$  values, where  $T_{1,surface}$  was calculated by the following restrictions: (i) only 0.4 ml fluid added samples are taken into consideration, (ii) for  $a$ , 0.25 nm as the silica layer thickness is assumed. As shown in **Table 7A**,  $T_{1,surface}$  values decreased as the temperature was increased only in the case of silica-4.0 nm and silica-1.5 nm. On the contrary, in the

case of silica-2.5 nm,  $T_{1,surface}$  values increased as the temperature was increased. This shows that water molecules form layers on the pore walls of silica-4.0 nm and silica-1.5 nm, and these layers have strong interaction with the pore walls. The contrary dynamical attitude of water in silica-2.5 nm is a reflection of the effect of surface-to-volume ratio. **Table 7B** shows that  $T_{1,surface}$  values of  $\text{CH}_3\text{OH}$  in the nanopores of silica-4.0 nm do not change significantly as a function of temperature. However, there is a systematic increase in  $T_{1,surface}$  values of  $\text{CH}_3\text{OD}$  in the nanopores of silica-4.0 nm when the temperature was elevated. This is attributed to the fluid chemistry.

Sattig et al. (2014) suggested that  $^2\text{H}$  NMR line-shape analysis evidenced pronounced dynamical heterogeneities for confined  $\text{H}_2\text{O}$ . In another study on characteristic properties of  $\text{H}_2\text{O}$  dynamical attitudes in confined forms explored by quasi-elastic

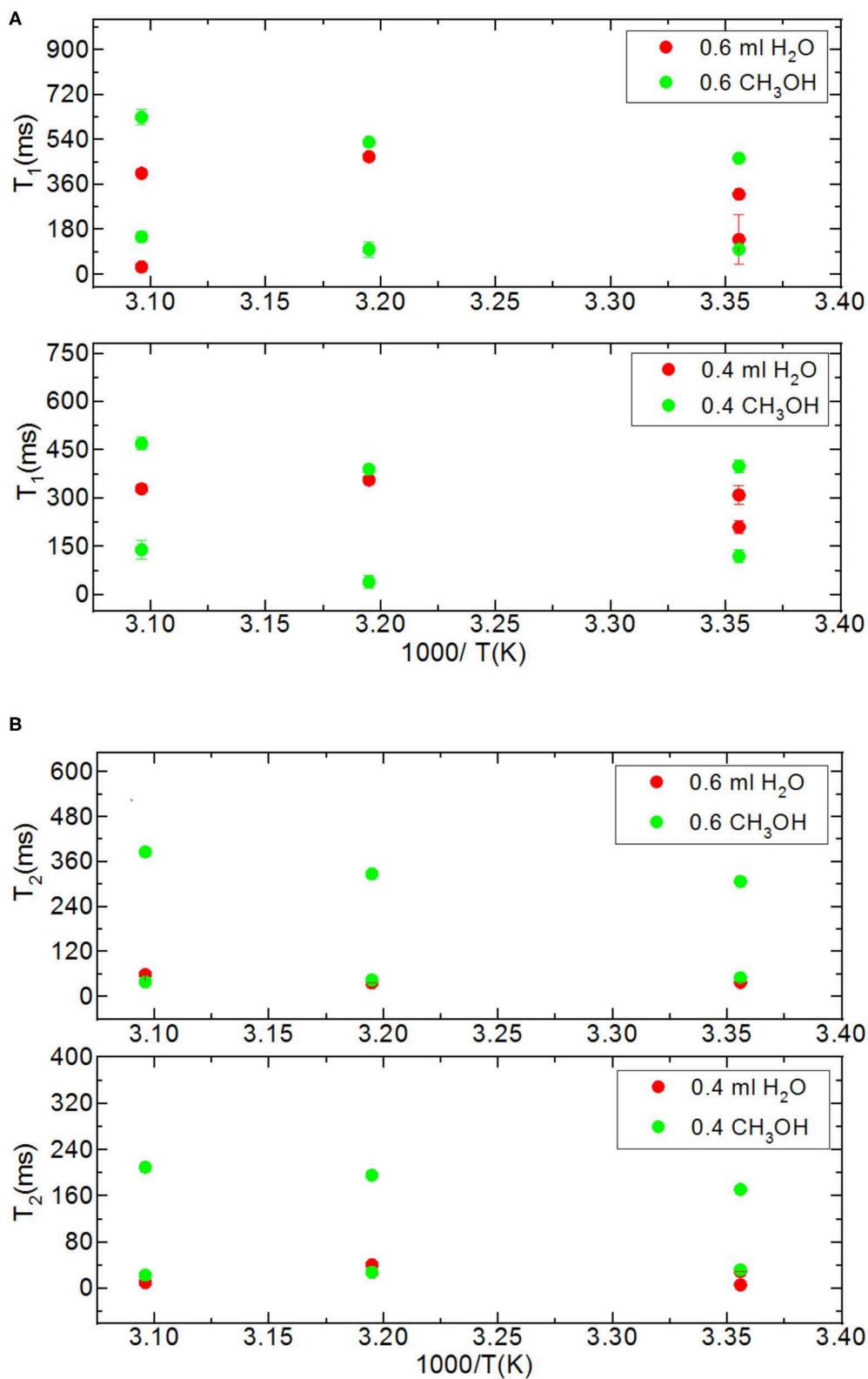


**FIGURE 4** | Comparison of relaxation values of H<sub>2</sub>O and CH<sub>3</sub>OH confined into silica-4.0 nm with the amount of 150 mg and S/V = 574 where the variables are temperature values (298, 313, and 323 K), and fluid-to-solid ratios (0.60 ml/150 mg, 0.40 ml/150 mg);  $T_1$  (A) and  $T_2$  (B).

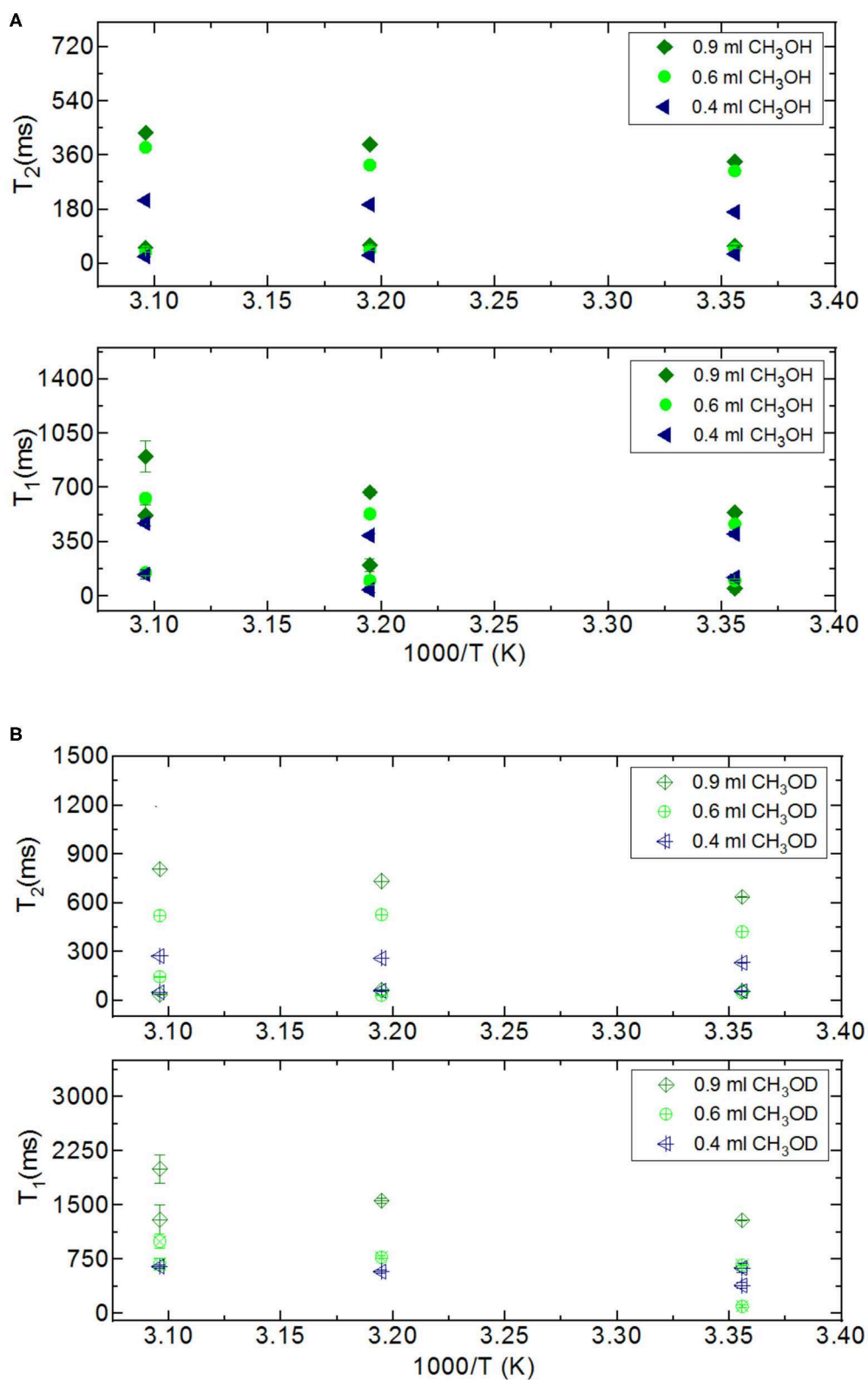
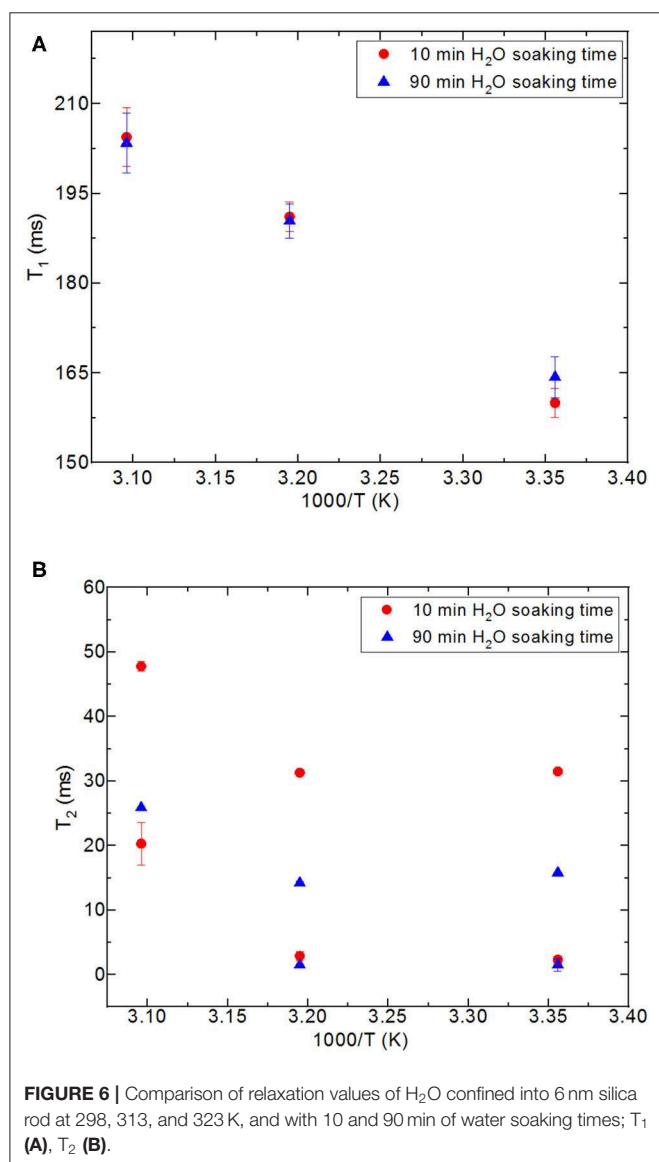


**FIGURE 5** | Comparison of relaxation values of CH<sub>3</sub>OH and CH<sub>3</sub>OD confined into silica-4.0 nm with the amount of 150 mg and S/V = 574 where the variables are temperature values (298, 313, and 323 K), and fluid-to-solid ratios (0.90 ml/150 mg, 0.60 ml/150 mg, 0.40 ml/150 mg); CH<sub>3</sub>OH **(A)**, CH<sub>3</sub>OD **(B)**.

**TABLE 6** |  $T_1$  and  $T_2$  values of water confined into nanoporous silica rod.

Silica_rod_6 nm			Silica_rod_6 nm		
Water soaking time 10 min			Water soaking time 90 min		
Temperature (°C)	$T_1$ (ms)	$T_2$ (ms)	Temperature (°C)	$T_1$ (ms)	$T_2$ (ms)
25	160 ± 2.4	31.5 ± 0.2 2.3 ± 0.6	25	164.3 ± 3.4	15.8 ± 0.1 1.5 ± 1.0
40	191.1 ± 2.5	31.3 ± 0.2 2.9 ± 0.7	40	190.4 ± 2.9	14.2 ± 0.2 1.5 ± 0.0
50	204.4 ± 4.9	47.8 ± 0.8 20.3 ± 3.3	50	203.4 ± 5.0	25.89 ± 0.1



neutron scattering, Osti et al. (2016) mentioned primary single parameter  $\theta$ , which is the ratio of the mean number of water molecules that are mostly affected by pore walls to the total

**TABLE 7A** |  $T_{1,surface}$  values of water in confined state.

	$T_{1,surface}$ (ms) with 0.4 ml water		
	25°C	40°C	50°C
Silica-4.0 nm	28.0	47.4	3.8
Silica-2.5 nm	842.7	909.4	1066.9
Silica-1.5 nm	263.0	182.0	44.2

**TABLE 7B** |  $T_{1,surface}$  values of CH<sub>3</sub>OH and CH<sub>3</sub>OD in confined state.

	$T_{1,surface}$ (ms): silica-4.0 nm + 0.4 ml fluid		
	25°C	40°C	50°C
CH <sub>3</sub> OH	15.6	5.1	18.2
CH <sub>3</sub> OD	55.5	86.3	98.3

number of H<sub>2</sub>O molecules under confinement. If we consider  $\theta$  as equal to a constant value such as (X) for a complete saturation with and without excess water by taking filling mechanism of MCM-41 with H<sub>2</sub>O mentioned by Grünberg et al. (2004) into account, we suggest that there are both  $\theta \approx X$  and  $\theta \leq X$  where there is dynamic exchange between confined water molecules (the ones not interacting with the pore walls) and the bulk excess water. For the samples with excess fluid as in the case of silica-4 nm,  $\theta$  for different fluid-solid-ratios is equal to each other. When the fluid-to-solid ratio is decreased for the partially filled samples,  $\theta$  also decreases down. Because  $\theta$  is utilized for the slit-type, cylindrical, and spherical geometries,  $\theta$  is applicable in the current study as well. Osti et al. (2016) used exact analytical techniques to explain H<sub>2</sub>O adsorption in three model geometries of slit-type, cylinder, and sphere to have deeper explanation of the change of  $\theta$  with the restricted geometry. In the present study, characterization of the engineered nanoporous proxies and the analysis of confined fluids are done in detail. For example, although nanoporous silica materials are known amorphous, degree of regular patterns of each sample was studied by XRD thoroughly to clarify the alignment and geometry of the pores.

A rough consideration of  $T_1/T_2$  ratios for both confined water and methanol clearly indicate a straightforward deducing

arrangement of comparative intensity of interaction with the pore uppermost layer of silica-4.0 nm: water has greater interaction with the pore surface than methanol (Weber et al., 2010; D'Agostino et al., 2012). For this reason, we think that methanol molecules establish clusters with extensive hydrogen bond formation in the pores rather than interacting with the pore surface (Tsotsalas et al., 2013). It was argued that the existence of porous medium disrupts the widespread intermolecular hydrogen-bonding system of some polyols such as glycerol and ethylene glycol, and this disruption in hydrogen bonding system resulted in boosted translation and tumbling movement degree, therefore longer  $T_1$  values. In our case, such a disruption might exist with respect to bulk liquids. However, this disruption is less effective for confined  $\text{CH}_3\text{OH}$  molecules than confined water molecules given that the same nanoporous matrix system is utilized for confining the molecules. In addition, we observe shorter  $T_1$  times for both of the confined fluids with respect to their bulk state. It is already known that NMR relaxation time values of confined fluids in porous media are relatively shorter than their corresponding fluids in bulk (Barrie, 2000). This situation is attributed to the uppermost layer and dipolar interactions and a decreased degree of reorientation of molecules at the pore uppermost layer (D'Agostino et al., 2012). We suggest these interactions dominate in terms of reducing the  $T_1$  times of both of the confined fluids.

In addition to comparing relaxation behaviors of confined  $\text{H}_2\text{O}$  and  $\text{CH}_3\text{OH}$ , we also compare relaxation behaviors of  $\text{CH}_3\text{OH}$  and  $\text{CH}_3\text{OD}$  under confinement. When we switch from  $\text{CH}_3\text{OH}$  to  $\text{CH}_3\text{OD}$ , we only measure confined behavior of  $-\text{CH}_3$  group. Both  $T_1$  and  $T_2$  of  $\text{CH}_3\text{OD}$  are longer than those of  $\text{CH}_3\text{OH}$ .  $T_1/T_2$  ratio of confined  $\text{CH}_3\text{OD}$  is also smaller as in the case of confined  $\text{CH}_3\text{OH}$ . This shows that there is weaker interaction between  $-\text{CH}_3$  and mesoporous silica-4.0 nm. Although confined  $\text{CH}_3\text{OD}$  behavior deviated from that of bulk  $\text{CH}_3\text{OD}$  upon confining into silica-4.0 nm, deviation is lesser than these of confined  $\text{H}_2\text{O}$  and  $\text{CH}_3\text{OH}$ . This also shows that hydrogen bonding capability of the molecules such as  $\text{H}_2\text{O}$  and  $\text{CH}_3\text{OH}$  with  $-\text{OH}$  groups decorating the pore walls influences both dynamics of the confined fluids and the layers formation on the pore walls.

## $T_2$ Distributions of Fluids Under Nanoporous Confinement

Figure 7 shows  $T_2$  distribution curves, obtained using Contin software, of  $\text{H}_2\text{O}$ ,  $\text{CH}_3\text{OH}$ , and  $\text{CH}_3\text{OD}$  confined in silica-4.0 nm. The distributed exponential approach utilizes a governing approach to the inverse Laplace transform yielding a continuous distribution of  $T_2$  relaxation times (Provencher, 1982). Mathematically speaking, the distributed exponential fitting is an ill-defined process because it is sensitive to the restrictions applied (Martens and Thybo, 2000; Hansen et al., 2010). Furthermore, there is a shorter  $T_2$  relaxation component observed in the range 10–15 ms. Such a component is mostly explained as a treating artifact due to the Contin processing stage (Aursand et al., 2008). For this reason, this component in

the  $T_2$  distributions is not taken into account in evaluating  $T_2$  distribution curves of the fluids confined into silica-4.0 nm.

In the case of the confined water inside silica-4.0 nm, when the fluid-to-solid ratio is lowered,  $T_2$  curves shifted toward shorter times. In addition,  $T_2$  curves became broader and had lower intensity (Figure 7A). On the other hand, confined  $\text{CH}_3\text{OH}$  has longer  $T_2$  components as seen in Figure 7B. The  $T_2$  curves with the highest intensities between 150 and 450 ms range exhibited the same tendency as in the case of confined water. In other words, lower fluid-to-solid ratio was reflected as lower intensity  $T_2$  distribution curves at shorter  $T_2$  times. For the range between 20 and 80 ms the same result was observed. However, line broadening in  $T_2$  distribution curves of confined  $\text{CH}_3\text{OH}$  was less pronounced. When the fluid-to-solid ratio was at the lowest value (0.4 ml  $\text{CH}_3\text{OH}$  confined to 150 mg silica 4.0 nm), there was a third  $T_2$  curve around 55 ms with broader distribution. When the fluid chemistry was switched to  $\text{CH}_3\text{OD}$ ,  $T_2$  distribution curves with the higher intensities were in the range between 100 and 900 ms. Consistently with the two other confined fluids, as the fluid-to-solid ratio was decreased,  $T_2$  curves shifted to shorter times with lower intensities. However, there were three  $T_2$  curves for each fluid-to-solid ratio. As the  $T_2$  curve shifts toward lower values, the  $T_2$  curve loses intensity. For this reason, the observation of three  $T_2$  curves for confined  $\text{CH}_3\text{OD}$  inside silica-4.0 nm might correspond to different proportions of the confined  $\text{CH}_3\text{OD}$  molecules (Bertram et al., 2002): (1) the ones forming layers on the pore walls by weak interactions with the  $-\text{OH}$  of the pore wall, (2) the ones closer to the middle of the pores and having lesser interactions with ones forming layers on the pore walls, (3) the ones clustering in the center of the pores. As reflected in longer  $T_2$  values, and continuous  $T_2$  distribution curves, among the three fluids of interest,  $\text{CH}_3\text{OD}$  has the weakest interaction with the pore walls.

## CONCLUSION

Specific pore volumes ( $\text{cm}^3/\text{g}$ ) of the nanoporous silica samples studied exhibit the following order: silica-1.5 nm > silica-4.0 nm > silica-2.5 nm. Nanopore diameter does not influence the dynamics of confined water significantly as revealed by the results on relaxation of water obtained by keeping pore volumes of porous matrixes constant for the given amounts of the porous materials. Rather than pore diameter, S/V ratio along with pore diameter reflects information on filling mechanism the nanopores with water. In the case of relatively larger pore diameter and small S/V ratio, wetting the surface of the nanopore walls is followed by additional filling from the pore wall to the midpoint of the pore until achieving complete filling of the pores (Grünberg et al., 2004). In the case of nanoporous silica with small pore diameter and large S/V ratio, the filling mechanism follows a different path: first, fluid fills the center of the pores leading to a co-presence of filled pore fragments with wetted pores. Further filling of the pores develops axially in the direction of the pore axis.

The possibility of distinguishing among relaxation times of excess and confined fluids, and to quantify excess fluid, fluid

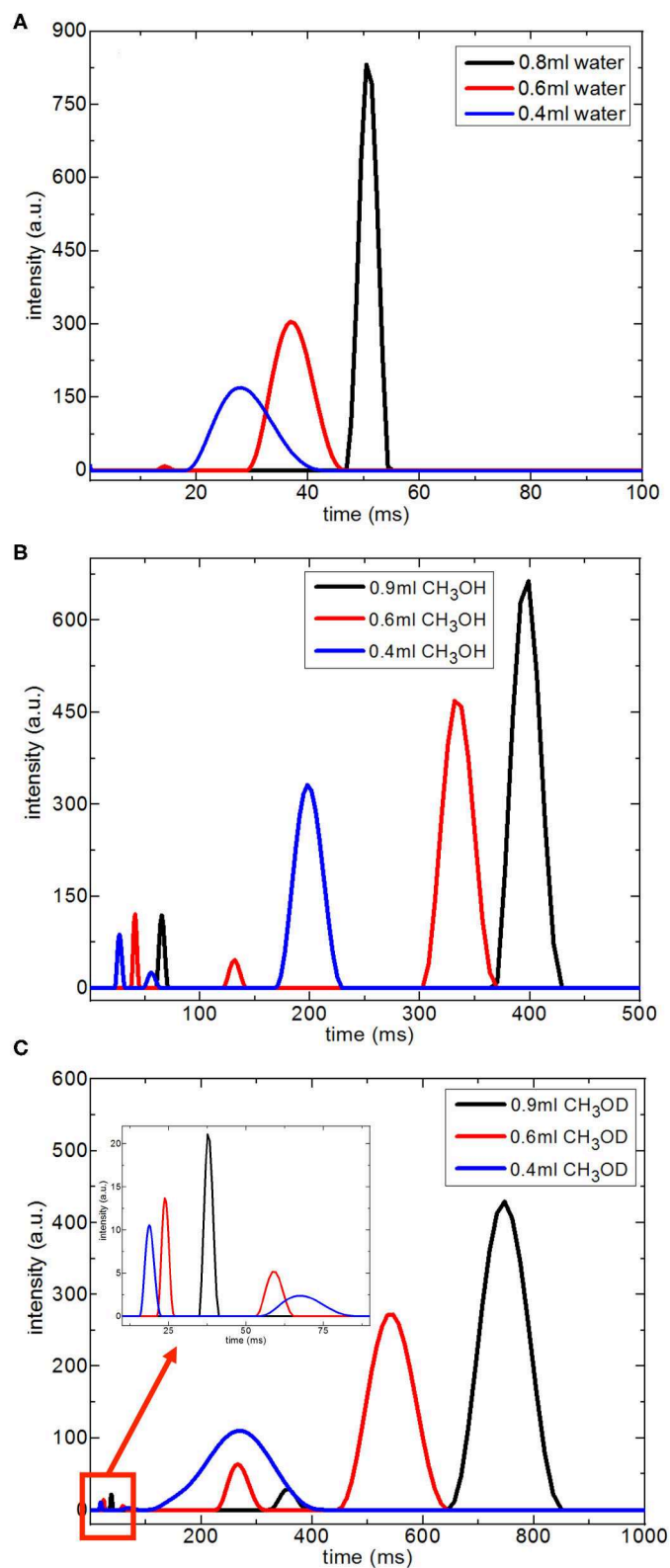


**FIGURE 7** | Continuous  $T_2$  relaxation time data for  $H_2O$  (A),  $CH_3OH$  (B), and  $CH_3OD$  (C) confined into silica-4.0 nm with the amount of 150 mg and  $SV = 574$  as a function of fluid-to-solid ratio.

found in the interparticle regions of nanoporous silica powder and outside the pores, and fluid confined in the nanopores of silica matrices might have applications in the petroleum industry, where characterization of rock with various pore sizes has significance for better definition of reservoirs. However, the highest S/V ratio leads to the longest  $T_1$  times of confined water, while the lowest S/V ratio resulted in the shortest  $T_1$  times of confined water. The decrease in  $T_2$  values as decreasing the fluid-to-solid ratio is more pronounced in the case of silica-2.5 nm having the lowest pore volume. These results clearly show the importance and influence of S/V ratio on dynamical behaviors of fluids confined into nanoporous proxies.

Comparison of  $T_1/T_2$  ratios, showing the affinity of the confined fluid to the pore walls, of both confined  $H_2O$  and  $CH_3OH$  clearly show that  $H_2O$  has stronger interaction with the pore surface of silica-4.0 nm than  $CH_3OH$ . The degree of deviation of confined  $CH_3OD$  behavior in silica-4.0 nm from that of bulk is less than those of confined  $H_2O$  and  $CH_3OH$ . It was claimed that a porous medium disrupts the extensive intermolecular hydrogen-bonding network of some polyols, and this disruption led to longer  $T_1$  values (D'Agostino et al., 2012). Such a disruption in hydrogen-bonding network is less effective for confined  $CH_3OH$  molecules than confined  $H_2O$  molecules for the same nanoporous matrix system. In addition to S/V ratio, chemistry of confined fluids also affects the dynamical measurements. This is an important observation, for example, in interpreting dynamical behaviors of confined and saturated mixtures of water and hydrocarbons at natural confined systems, where wettability alteration occurring inside the porous structures of the rocks influences the crude oil production.

The continuous  $T_2$  distribution curves suggest that weaker interaction between  $CH_3OD$  and nanoporous silica-4.0 nm with three different environments: (i) layered structure by weak interactions with the pore walls, (ii) the ones closer to the center of pores and interacting weakly with the first layer on the pore wall, (iii) the ones forming cluster in the middle of the nanopores.

Finally, the characteristics and properties of the nanoporous matrix systems are defined in a better way. Furthermore, low-field  $^1H$  NMR is a powerful technique when exploring confined fluid dynamics as a function of the aforementioned

parameters. These nanoporous silica samples are ideal examples that mimic the natural geological systems such as heterogeneous subsurface materials containing crude oil and brine solutions to mimic nano-environments present in natural systems such as rocks. Based on the findings on the properties of mesoporous silica proxies and dynamical behavior of confined crude oil and brine confined into mesoporous silica materials, we also analyzed sandstone rock cores flooded with crude oil and brine with hydrophobic/oleophilic nanoparticles in addition to characterizing natural carbonate rock cores saturated with water and crude oil. The results of these measurements are to be discussed in forthcoming publications.

## DATA AVAILABILITY STATEMENT

All datasets generated for this study are included in the article/**Supplementary Material**.

## AUTHOR CONTRIBUTIONS

SO planned and conducted the low-field NMR measurements in addition to TGA measurements. BH contributed to the low-field NMR measurements. TL completed the BET and TXRD measurements. JS and SW contributed to each and every step of the study, and in particular on both TXRD and BET parts. K-HL and C-YM synthesized silica-2.5 nm and silica-1.5 nm. DC was the research leader. All authors contributed to the article and approved the submitted version.

## FUNDING

Support for SO was provided by the A.P. Sloan Foundation sponsored Deep Carbon Observatory. DC, JS, and SW were supported by the Department of Energy, Basic Energy Sciences Geosciences Program under grant DE-SC0006878.

## SUPPLEMENTARY MATERIAL

The Supplementary Material for this article can be found online at: <https://www.frontiersin.org/articles/10.3389/fchem.2020.00734/full#supplementary-material>

## REFERENCES

- Al-Othman, Z. A. (2012). A review: fundamental aspects of silicate mesoporous materials. *Materials* 5, 2874–2902. doi: 10.3390/ma5122874
- Asefa, T., and Tao, Z. (2012). Mesoporous silica and organosilica materials-review of their synthesis and organic functionalization. *Can. J. Chem.* 90, 1015–1031. doi: 10.1139/v2012-094
- Aursand, I. G., Gallart-Jornet, L., Erikson, U., Axelson, D. E., and Rustad, T. (2008). Water distribution in brine salted cod (*Gadus morhua*) and aalmon (*Salmo salar*): a low-field  $^1H$  NMR study. *J. Agric. Food Chem.* 56, 6252–6260. doi: 10.1021/jf800369n
- Barrie, P. J. (2000). Characterization of porous media using NMR methods. *Annu. Rep. NMR Spectrosc.* 41, 265–316. doi: 10.1016/S0066-4103(00)41011-2
- Barut, G., Pissis, P., Pelster, R., and Nimtz, G. (1998). Glass transition in liquids: two versus three-dimensional confinement. *Phys. Rev. Lett.* 79, 3543–3546. doi: 10.1103/PhysRevLett.80.3543
- Bellissent-Funel, M.-C., Chen, S. H., and Zanotti, J. M. (1995). Single-particle dynamics of water molecules in confined space. *Phys. Rev. E* 51, 4558–4569. doi: 10.1103/PhysRevE.51.4558
- Bergman, R., and Swenson, J. (2000). Dynamics of supercooled water in confined geometry. *Nature* 403, 283–285. doi: 10.1038/35002027
- Bertram, H. C., Purslow, P. P., and Andersen, H. J. (2002). Relationship between meat structure, water mobility, and distribution: a low-field nuclear magnetic resonance study. *J. Agric. Food Chem.* 50, 824–829. doi: 10.1021/jf010738f
- Bhattacharya, S., D'Orazio, F., Tarczon, J. C., Halperin, W. P., and Gerhardt, R. (1989). Internal structure of porous silica: a model system for characterization

- by nuclear magnetic resonance. *J. Am. Ceram. Soc.* 72, 2126–2130. doi: 10.1111/j.1151-2916.1989.tb06043.x
- Bloembergen, N., Purcell, E. M., and Pound, R. V. (1948). Relaxation effects in nuclear magnetic resonance absorption. *Phys. Rev.* 73, 679–746. doi: 10.1103/PhysRev.73.679
- Bruni, F., Ricci, M. A., and Soper, A. K. (1998). Water confined in vycor glass. I. A neutron diffraction study. *J. Chem. Phys.* 109, 1478–1485. doi: 10.1063/1.476698
- Buntkowsky, G., Breitzke, H., Adamczyk, A., Roelofs, F., Emmeler, T., Gedat, E., et al. (2007). Structural and dynamical properties of guest molecules confined in mesoporous silica materials revealed by NMR. *Phys. Chem. Chem. Phys.* 9, 4843–4853. doi: 10.1039/b707322d
- D'Agostino, C., Mitchell, J., Gladden, L. F., and Mantle, M. D. (2012). Hydrogen bonding network disruption in mesoporous catalyst supports probed by PFG-NMR diffusometry and NMR relaxometry. *J. Phys. Chem. C* 116, 8975–8982. doi: 10.1021/jp2123295
- Denisov, V., and Halle, B. (1996). Protein hydration dynamics in aqueous solution. *Faraday Discuss.* 103, 227–244. doi: 10.1039/fd9960300227
- D'Orazio, F., Bhattaharja, S., Halperin, W. P., Eguchi, K., and Mizusaki, T. (1990b). Molecular diffusion and nuclear-magnetic-resonance relaxation of water in unsaturated porous silica glass. *Phys. Rev. B* 42, 9810–9818. doi: 10.1103/PhysRevB.42.9810
- D'Orazio, F., Bhattaharja, S., Halperin, W. P., and Gerhardt, R. (1990a). Fluid transport in partially filled porous sol-gel silica glass. *Phys. Rev. B* 42, 6503–6508. doi: 10.1103/PhysRevB.42.6503
- Gallegos, D. P., Smith, D. M., and Brinker, C. J. (1988). An NMR technique for the analysis of pore structure: application to mesopores and micropores. *J. Coll. Inter. Sci.* 124, 186–198. doi: 10.1016/0021-9797(88)90339-6
- Grünberg, B., Emmeler, T., Gedat, E., Shenderovich, I., Findenegg, G. H., Limbach, H.-H., et al. (2004). Hydrogen bonding of water confined in mesoporous silica MCM-41 and SBA-15 studied by  $^1\text{H}$  solid-state NMR. *Chem. Eur. J.* 10, 5689–5696. doi: 10.1002/chem.200400351
- Hansen, C. L., Thybo, A. K., Bertram, H. C., Viereck, N., van den Berg, F., and Engelsen, S. B. (2010). Determination of dry matter content in potato tubers by low-field nuclear magnetic resonance (LF-NMR). *J. Agric. Food Chem.* 58, 10300–10304. doi: 10.1021/jf101319q
- Kapur, G. S., Findeisen, M., and Berger, S. (2000). Analysis of hydrocarbon mixtures by diffusion-ordered NMR spectroscopy. *Fuel* 79, 1347–1351. doi: 10.1016/S0016-2361(99)00271-9
- Liu, K.-H., Zhang, Y., Lee, J.-J., Chen, C.-C., Yeh, Y.-Q., Chen, S.-H., et al. (2013). Density and anomalous thermal expansion of deeply cooled water confined in mesoporous silica investigated by synchrotron x-ray diffraction. *J. Chem. Phys.* 139, 064502. doi: 10.1063/1.4817186
- Liu, L., Chen, S. H., Faraone, A., Yen, C. W., Mou, C. Y., Kolesnikov, A. I., et al. (2006). Quasielastic and inelastic neutron scattering investigation of fragile-to-strong crossover in deeply supercooled water confined in nanoporous silica matrices. *J. Phys. Condens. Matter* 18, S2261–S2284. doi: 10.1088/0953-8984/18/36/S03
- Liu, Y., Zhang, W. Z., and Pinnavaia, T. J. (2000). Steam-stable aluminosilicate mesostructures assembled from zeolite type Y seeds. *J. Am. Chem. Soc.* 122, 8791–8792. doi: 10.1021/ja001615z
- Macomber, R. S. (1998). *A Complete Introduction to Modern NMR Spectroscopy*. New York, NY: John Wiley and Sons, Inc.
- Mallamace, F., Corsaro, C., Mallamace, D., Vasi, S., Vasi, C., and Stanley, H. E. (2014). Thermodynamic properties of bulk and confined water. *J. Chem. Phys.* 141:18C504. doi: 10.1063/1.4895548
- Martens, H. J., and Thybo, A. K. (2000). An integrated microstructural, sensory and instrumental approach to describe potato texture. *LWT Food Sci. Technol.* 33, 471–482. doi: 10.1006/fstl.2000.0688
- Millischuk, A. A., and Ladanyi, B. M. (2011). Structure and dynamics of water confined in silica nanopores. *J. Chem. Phys.* 135:174709. doi: 10.1063/1.3657408
- Millischuk, A. A., and Ladanyi, B. M. (2014). Polarizability anisotropy relaxation in nanoconfinement: molecular simulation study of water in cylindrical silica nanopores. *J. Chem. Phys.* 141, 18C513-1–18C513-9. doi: 10.1063/1.4896218
- Mitchell, J., Hurlimann, M. D., and Fordham, E. J. (2009). A rapid measurement of T1/T2: the DECPMG sequence. *J. Magn. Reson.* 200, 198–206. doi: 10.1016/j.jmr.2009.07.002
- Nicotera, I., Angjeli, K., Coppola, L., Arico, A. S., and Baglio, V. (2012). NMR and electrochemical investigation of the transport properties of methanol and water in nafion and clay-nanocomposites membranes for DMFCs. *Membranes* 2, 325–345. doi: 10.3390/membranes2020325
- Ok, S., Hoyt, D. W., Andersen, A., Sheets, J., Welch, S. A., Cole, D. R., et al. (2017). Surface interactions and confinement of methane: a high pressure magic angle spinning NMR and computational chemistry study. *Langmuir* 33, 1359–1367. doi: 10.1021/acs.langmuir.6b03590
- Osti, N. C., Cote, A., Mamontov, E., Ramirez-Cuesta, A., Wesolowski, D. J., and Diallo, S. O. (2016). Characteristic features of water dynamics in restricted geometries investigated with quasi-elastic neutron scattering. *Chem. Phys.* 465–466, 1–8. doi: 10.1016/j.chemphys.2015.11.008
- Provencher, S. W. (1982). A constrained regularization method for inverting data represented by linear algebraic of integral equations. *Comput. Phys. Commun.* 27, 213–227. doi: 10.1016/0010-4655(82)90173-4
- Ricci, M. A., and Rovere, M. (2000). Studies of water in confinement by experiments and simulations. *J. Phys.* 10, 187–193. doi: 10.1051/jp4:2000737
- Sarawade, P. B., Shao, G. N., Quang, D. V., and Kim, H. T. (2013). Effect of various structure directing agents on the physicochemical properties of the silica aerogels prepared at an ambient pressure. *Appl. Surf. Sci.* 287, 84–90. doi: 10.1016/j.apsusc.2013.09.072
- Sattig, M., Reutter, S., Fujara, F., Werner, M., Buntkowsky, G., and Vogel, M. (2014). NMR studies on the temperature-dependent dynamics of confined water. *Phys. Chem. Chem. Phys.* 16, 19229–19240. doi: 10.1039/C4CP02057J
- Sindorf, D. W., and Maciel, G. E. (1983). Silicon-29 NMR study of dehydrated/rehydrated silica gel using cross polarization and magic-angle spinning. *J. Am. Chem. Soc.* 105, 1487–1493. doi: 10.1021/ja00344a012
- Sing, K. S. W., Everett, D. H., Haul, R. A. W., Moscou, L., Pierotti, R. A., Rouquerol, J., et al. (1985). Reporting physisorption data for gas–solid systems. *Pure Appl. Chem.* 57, 603–619. doi: 10.1351/pac198557040603
- Slichter, C. P. (1990). *Principles of Magnetic Resonance, 3rd Edn.* New York, NY: Springer Series in Solid State Science. doi: 10.1007/978-3-662-09441-9
- Steytler, D. C., and Dore, J. C. (1985). Neutron diffraction studies of water in porous silica. *Mol. Phys.* 56, 1001–1015. doi: 10.1080/00268978500102851
- Swenson, J., Bergman, R., and Longeville, S. (2001). A neutron spin-echo study of confined water. *J. Chem. Phys.* 115, 11299–11305. doi: 10.1063/1.1420728
- Tangestaninejad, S., Moghadam, M., Mirkhani, V., Baltork, I. M., and Ghani, K. (2009). Alkene epoxidation catalyzed by molybdenum supported on functionalized MCM-41 containing N–S chelating Schiff base ligand. *Catal. Commun.* 10, 853–858. doi: 10.1016/j.catcom.2008.12.010
- Thommes, M., Kaneko, K., Neimark, A. V., Olivier, F. R.-R., Rouquerol, J., and Sing, K. S. W. (2015). Physisorption of gases, with special reference to the evaluation of surface area and pore size distribution, IUPAC Technical Report. *Pure Appl. Chem.* 87, 1051–1069. doi: 10.1515/pac-2014-1117
- Timur, A. (1969). Pulsed nuclear magnetic resonance studies of porosity, movable fluid, and permeability of sandstones. *J. Petrol. Technol.* 21, 775–786. doi: 10.2118/2045-PA
- Tsotsalas, M., Hejcik, P., Sumida, K., Kalay, Z., Furukawa, S., and Kitagawa, S. (2013). Impact of molecular clustering inside nanopores on desorption processes. *J. Am. Chem. Soc.* 135, 4608–4611. doi: 10.1021/ja312115x
- Vogel, M. (2010). NMR studies on simple liquids in confinement. *Eur. Phys. J.* 189, 47–64. doi: 10.1140/epjst/e2010-01309-9
- Webber, B., and Dore, J. (2004). Structural and dynamic studies of water in mesoporous silicas using neutron scattering and nuclear magnetic resonance. *J. Phys. Condens. Matter* 16, S5449–S5470. doi: 10.1088/0953-8984/16/45/009
- Weber, D., Mitchell, J., McGregor, J., and Gladden, L. F. (2009). Comparing strengths of surface interactions for reactants and solvents in porous catalysts

- using two-dimensional NMR relaxation correlations. *J. Phys. Chem. C* 113, 6610–6615. doi: 10.1021/jp811246j
- Weber, D., Sederman, A. J., Mantle, M. D., Mitchell, J., and Gladden, L. F. (2010). Surface diffusion in porous catalysts. *Phys. Chem. Chem. Phys.* 12, 2619–2624. doi: 10.1039/b921210h
- Wu, D., and Navrotsky, A. (2013). Small molecule-silica interactions in porous silica structures. *Geochim. Cosmochim. Acta* 109, 38–50. doi: 10.1016/j.gca.2013.01.038
- Zanotti, J. M., Bellissent-Funel, M.-C., and Chen, S. H. (1999). Relaxational dynamics of supercooled water in porous glass. *Phys. Rev. E* 59, 3084–3093. doi: 10.1103/PhysRevE.59.3084

**Conflict of Interest:** The authors declare that the research was conducted in the absence of any commercial or financial relationships that could be construed as a potential conflict of interest.

Copyright © 2020 Ok, Hwang, Liu, Welch, Sheets, Cole, Liu and Mou. This is an open-access article distributed under the terms of the Creative Commons Attribution License (CC BY). The use, distribution or reproduction in other forums is permitted, provided the original author(s) and the copyright owner(s) are credited and that the original publication in this journal is cited, in accordance with accepted academic practice. No use, distribution or reproduction is permitted which does not comply with these terms.